Campanian-Eocene dinoflagellate cyst biostratigraphy in the Southern Andean foreland basin: Implications for Drake Passage throughflow

*Peter K. Bijl[1], G. Raquel Guerstein[2], Edgar A. Sanmiguel Jaimes[3], Appy Sluijs[1],
Silvio Casadio[4], Víctor Valencia[5], Cecilia R. Amenábar[6], Alfonso Encinas[7]

[1] *Department of Earth Sciences, Laboratory of Palaeobotany and Palynology, Utrecht University, Heidelberglaan 8, 3584 CS Utrecht*
  The Netherlands .
  p.k.bijl@uu.nl; A.sluijs@uu.nl

[2] *Departamento de Geología, Universidad Nacional del Sur-Instituto Geológico del Sur, CONICET, Av. Alem 1253, cuerpo B´-2° Piso*
  Argentina.
  raquel.guerstein@uns.edu.ar

[3] *Universidad Andres Bello, Facultad de Ingenieria, Autopista Concepción-Talcahuano, 7100 Talcahuano, Chile.*
  geosanmiguel@hotmail.com

[4] *Universidad Nacional de Río Negro, Instituto de Investigación en Paleobiología y Geología, Av. Roca 1242, General Roca, Río*
  Negro, Argentina.
  scasadio@unrn.edu.ar

[5] *School of the Environment, Washington State University, Pullman, WA 99163, USA.*
  victorv@email.arizona.edu

[6] *Instituto Antártico Argentino-Instituto de Estudios Andinos Don Pablo Groeber-CONICET-Dpto. Ciencias Geológicas, Universidad*
  de Buenos Aires, Intendente Guiraldes 2160, C1428EGA, Ciudad Universitaria, Argentina.
  cr_amenabar@yahoo.com.ar

[7] *Departamento de Ciencias de la Tierra, Facultad de Ciencias Químicas, Universidad de Concepción, Edmundo Larenas 129, casilla*
  160-C, Concepción, Chile.
  alfonso.encinas@gmail.com

(*) Corresponding author: p.k.bijl@uu.nl

ABSTRACT. The tectonic opening of the Tasmanian Gateway and Drake Passage represented crucial geographic requirements for the Cenozoic development of the Antarctic Circumpolar Current (ACC). Particularly the tectonic complexity of Drake Passage has hampered the exact dating of the opening and deepening phases, and the consequential onset of throughflow of the ACC. One of the obstacles is putting key regional tectonic events, recorded in southern Patagonian sediments, in absolute time. For that purpose, we have collected Campanian-Eocene sediment samples from the Chilean sector of Southern Patagonia. Using U-Pb radiometric dating on zircons and dinoflagellate cyst biostratigraphy, we updated age constraints for the sedimentary formations, and the hiatuses in between. Thick sedimentary packages of shallow-marine and continental sediments were deposited in the foreland basin during the early Campanian, mid-Paleocene, the Paleocene-Eocene boundary interval and the middle Eocene, which represent phases of increased foreland subsidence. We interpret regional sedimentary hiatuses spanning the late Campanian, early-to mid-Paleocene, mid-Eocene and latest Eocene-early Oligocene to indicate times of reduced foreland subsidence, relative to sediment supply. We relate these changes to varying subduction rates and Andean orogeny. Dinoflagellate cyst assemblages suggest that the region was under the influence of the Antarctic-derived waters through the western boundary current of the Subpolar Gyre, developed in the southwest Atlantic Ocean and thus argues for limited throughflow through the Drake Passage until at least the latest Eocene. However, the proliferation of dinoflagellate endemism we record in the southwest Atlantic is coeval with that in the southwest Pacific, and on a species level, dinoflagellate cyst assemblages are the same in these two regions. This suggests that both regions were oceanographically connected throughout the early Paleogene, likely through a shallow opening of a restricted Drake Passage. This implies a continuous surface-water connection between the south Pacific and the South Atlantic throughout the late Cretaceous-early Paleogene.

Keywords: Dinoflagellate cysts, Biostratigraphy, Radiometric dating, Drake Passage, Paleoceanography, Endemism.

RESUMEN. Bioestratigrafía de quistes dinoflagelados del Campaniano-Eoceno en la cuenca de antepaís de los Andes meridionales: implicancias para la circulación oceánica a través del Pasaje de Drake. La apertura tectónica del Conducto de Tasmania y del Pasaje de Drake implicó dos requisitos geográficos cruciales para el desarrollo de la Corriente Circumpolar Antártica (CCA) durante el Cenozoico. En particular, la complejidad tectónica del Pasaje de Drake ha dificultado la datación precisa de las fases de apertura y profundización, y el consiguiente inicio del flujo de la CCA. Uno de los problemas es poner en tiempo absoluto los eventos tectónicos regionales claves, registrados en los sedimentos del sur de la Patagonia. Para ese propósito, recolectamos muestras de sedimentos del Campaniano-Eoceno del sector chileno de la Patagonia meridional. Utilizando la datación radiométrica de U-Pb en circones y la bioestratigrafía de quistes de dinoflagelados (dinoquistes), actualizamos los límites de edades de las formaciones sedimentarias, y los hiatos entre ellas. Los espesos paquetes sedimentarios de sedimentos marinos poco profundos y continentales fueron depositados durante el Campaniano temprano, el Paleoceno medio, el límite Paleoceno-Eoceno y el Eoceno medio, que representan fases de mayor subsidencia de la cuenca. Interpretamos la existencia de hiatos sedimentarios regionales que abarcan el Campaniano tardío, el Paleoceno temprano y medio, el Eoceno medio y el Eoceno tardío-Oligoceno temprano para indicar los momentos de menor subsidencia del terreno en relación con el aporte de sedimentos. Vinculamos estos cambios con la variación de las tasas de subducción y la orogenia andina. Las asociaciones de dinoquistes sugieren que la región estaba bajo la influencia de aguas provenientes de la Antártica a través de la corriente de borde occidental del Giro Subpolar desarrollado en el Atlántico sudoccidental y, por lo tanto, argumentan a favor de un flujo limitado a través del Pasaje de Drake hasta por lo menos el Eoceno más tardío. Sin embargo, la proliferación del endemismo de dinoflagelados que registramos en el Atlántico sudoccidental es coetánea con la del Pacífico sudoccidental, y a nivel de especies, se caracterizan por las mismas asociaciones de dinoquistes. Esto sugiere que ambas regiones estaban conectadas durante el Paleógeno temprano, probablemente a través de una apertura somera en un Pasaje de Drake limitado. Esto implica una conexión continua de agua superficial entre el Pacífico Sur y el Atlántico Sur durante el Cretácico tardío-Paleógeno temprano.

Palabras clave: Quistes de dinoflagelados, Bioestratigrafía, Datación radiométrica, Pasaje de Drake, Paleoceanografía, Endemismo.

1. Introduction

The Antarctic Circumpolar Current (ACC), the largest and strongest ocean current on our planet, is one of the main drivers of global deep ocean circulation and mid- to high latitude climate of the southern hemisphere (Orsi *et al*., 1995). It remains unclear when the ACC first developed, attained its present-day strength and how its evolution influenced Antarctic and global climates (*e.g*., Barker *et al*., 2007). The continental conduit at Drake Passage (Fig. 1) was a major geographical barrier that prevented circumpolar ocean circulation for a large portion of the Cenozoic (Barker and Thomas, 2004), and as such has long represented a key study area to understand the development of the ACC (*e.g*., Sijp *et al*., 2014). Several challenges prevent a clear understanding the timing and evolution of the opening of Drake Passage. First, the Drake Passage area represents a series of oceanic basins, spreading- and subduction zones and continental micro-blocks, which makes tectonic restoration a complex puzzle (Lagabrielle *et al.*, 2009; Pérez *et al*., 2019). Second, these micro-blocks likely underwent a series of submersion and uplifting phases, which makes recurring obstruction and re-opening of Drake Passage a possibility. Third, the sedimentary

sequences that document the tectonic evolution of the region are notoriously difficult to date: carbonate and silica microfossils are not well preserved.

The Scotia Sea separates the Antarctic Peninsula from South America (Fig. 1) and contains several (at present-day) submerged continental blocks that were separated from the American and west-Antarctic plates in the process of rifting. Between these blocks, oceanic crust formed along a number of mid-ocean ridges (Lagabrielle *et al*., 2009; Pérez *et al*., 2019). Continental extension likely started prior to the early-middle Eocene boundary (~49 Ma; Livermore *et al*., 2005; Lagabrielle *et al*., 2009) and ocean crust formed from the late Eocene onwards (Eagles and Livermore, 2002). These tectonic reconstructions provide little constraint on the bathymetric depths of submerged continental blocks, and therefore the question remains whether or not there was shallow ocean throughflow during the Cretaceous-early Paleogene.

As an alternative approach, oceanographic changes around Drake Passage have been investigated as a "smoking gun" for Drake Passage opening and onset of the ACC. Scher and Martin (2006) suggested bottom water connectivity between the South Atlantic and South Pacific from 41 Ma onwards based on Neodymium isotope ratios. Whilst such reconstructions
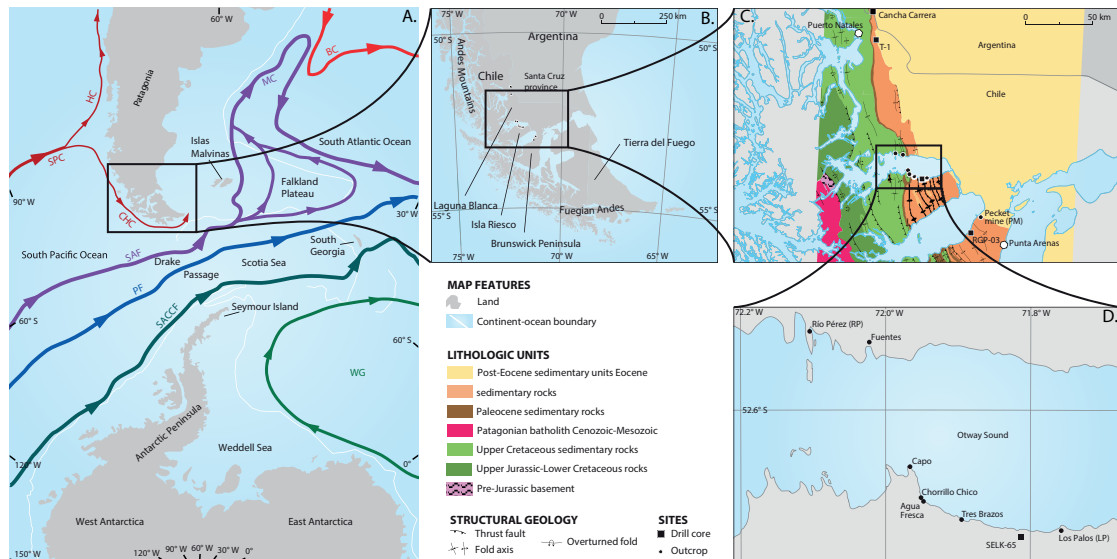
FIG. 1. Location map of studied sites. **A.** Geographic map of the Drake Passage area. White lines depict continent-ocean boundaries. Colored lines schematically depict prevailing ocean surface currents. **WG:** Weddell Gyre, **SACCF:** Southern ACC Front, **PF:** Polar Front, **SAF:** Subantarctic Front, **CHC:** Cape Horn Current, **HC:** Humboldt Current, **SPC:** South Pacific Current, **MC:** Malvinas Current, **BC:** Brazil Current. **B.** Detailed map of Southern Patagonia and Tierra del Fuego. **C.** Detailed map of the Brunswick Peninsula area, showing lithostratigraphic units and geologic structures (based on Sernageomin, 2003). **D.** Detailed map of the Otway Sound area, showing the localities of the sample sites on North shore of Isla Riesco and Fuentes/ Río Pérez outcrops.

do not reach beyond the mid-Eocene, more recent tectonic studies do interpret renewed compression in the Drake Passage region during the Oligocene (Lagabrielle *et al.*, 2009), with potential for temporal restriction of the Drake Passage following initial Eocene opening. Indeed, while oceanic basins existed in the Scotia Sea since the late Eocene, the greatest unknown, and crucial for an unrestricted flow of an incipient ACC, is the height and exact position of the continental micro-blocks that formed a barrier. This leaves the details of Drake Passage opening as yet poorly understood.

Studies on the Tasmanian Gateway have shown the potential of dinoflagellate cyst-based oceanographic reconstructions for understanding the history of Southern Ocean gateways (*e.g.*, Huber *et al.*, 2004; Bijl *et al.*, 2011). Dinoflagellate cysts show strict provincialism on either side of the Tasmanian Gateway prior to opening: cosmopolitan and low-latitude derived assemblages west of the Gateway, in the Australo-Antarctic Gulf (Brinkhuis *et al.*, 2003a; Bijl *et al.*, 2011; Houben *et al.*, 2019) and Antarctic-endemic assemblages in the southwest Pacific, east of the Gateway (Bijl *et al.*, 2011, 2013a).

The continued widening of the Australo-Antarctic Gulf allowed eastward progression of the proto-Leeuwin Current towards the still closed Tasmanian Gateway (Sauermilch *et al.*, 2019). The earliest signs of Tasmanian Gateway opening come from the appearance of endemic dinoflagellate cyst species on the Antarctic margin on the western side of the gateway, which indiciates throughflow of a westward counter current along the Antarctic margin into the Australo-Antarctic Gulf by the end of the early Eocene, 49 Ma (Bijl *et al.*, 2013a). Coarse-resolution ocean model simulations suggest that this westward counter current was relatively weak and only present with a closed Drake Passage (Sijp *et al.*, 2016), although this result is strongly dependent on the insufficiently constrained regional geographic and climatic boundary conditions.

A second phase of opening widened and seemingly deepened the Tasmanian Gateway from around 35 Ma onwards, which had great consequences for regional ocean current configuration. Throughflow of a proto-ACC was induced (Sluijs *et al.*, 2003; Stickley *et al.*, 2004), and surface currents accelerated (Houben *et al.*, 2019). Numerical model simulations

by Sijp *et al.* (2016) suggest this could only have occurred if Drake Passage was sufficiently deep as well (~350 m in the model simulation). Thus, these simulations imply that with both gateways open, the subpolar cyclonic gyres were disrupted by an incipient unrestricted ACC and the endemic assemblage became extinct (Huber *et al.*, 2004; Guerstein *et al.*, 2010; Bijl *et al.*, 2011). However, progressive cooling of the Southern Ocean may have played an additional role (Houben *et al.*, 2019).

With the development of the Tasmanian Gateway now relatively well-constrained, improved understanding is needed of the tectonic developments of Drake Passage. For Drake Passage, however, the microfossil evidence supporting this oceanographic regime is thus far insufficient. Evidence for the oceanographic consequences of Drake Passage opening can only come from sediments from the Atlantic side (*e.g.*, Guerstein *et al.*, 2010, 2014; Houben *et al.*, 2019) and the Antarctic Peninsula (*e.g.*, Douglas *et al.*, 2014; Amenábar *et al.*, 2019), as sediments from the Pacific side have been lost through subduction.

The Andean orogeny has created foreland basins with deep depocentres, and subsequent uplift has exposed these Campanian-Eocene sedimentary successions. Previous work on Eocene outcrops in the Santa Cruz and Tierra del Fuego provinces in the Austral Basin, Argentina, has documented a dominant Antarctic endemic dinoflagellate cyst community during the middle Eocene there as well (Guerstein *et al.*, 2010, 2014; González Estebenet *et al.*, 2016). However, the start of the proliferation of this endemic-Antarctic community in the southwest Atlantic Ocean and how this relates to regional oceanography remain unclear. In addition, the general scarcity of data implies that better spatial coverage of longer and more complete records can shed new light on the details of tectonic and oceanographic developments in the region.

Therefore, we studied a series of shallow-marine late Cretaceous-Eocene rocks from the Chilean Patagonia region. We analyzed outcrop and core samples from three regions: Laguna Blanca region, Isla Riesco and the Brunswick Peninsula (Fig. 1). The sedimentary rocks are from basin depocenters and thus supposedly correspond to the deepest possible depositional settings, where the potential for continuous sedimentation is the highest. We provide a coherent and detailed chronostratigraphic framework for the sequences through dinoflagellate cyst biostratigraphy,

taking advantage of the well-calibrated dinoflagellate cyst bioevents for the Southern Ocean (*e.g.*, Bijl *et al.*, 2013b; González Estebenet *et al.*, 2016; Fig. 2), and radiometric dating of zircons. Dinoflagellate cyst assemblages are subsequently used to assess depositional setting (Sluijs *et al.*, 2005; Frieling and Sluijs, 2018) and the degree of endemism (Bijl *et al.,* 2011). This allows us to reconstruct the oceanographic regime in the Southwest Atlantic and compare it to that of Tasmanian region, thereby inferring the oceanographic connectivity through Drake Passage.

2. Material

2.1. Sample collection

The samples for this study were collected in January 2016. We sampled outcrops and core material in three regions: Laguna Blanca, Isla Riesco and Brunswick Peninsula (Fig. 1; Table 1). For exact locations of our sampling, the global positioning system coordinates are available upon request. We preferentially sampled fine-grained intervals rather than coarse-grained sandstones, in order to optimize chances of well-preserved organic microfossil yields. Sample sites were cleared of weathered material but some influence of post-depositional weathering cannot be excluded. Core material recovered was made available by Ingeniería Civil Vicente (ICV), was photographed prior and after sampling (photos available upon request). We systematically took 3 samples per 1.5 meter-long core section, again with the exception of coarse-grained sandstone intervals. The drilled depth intervals for the cores, as marked on the core boxes and our measurements of the lengths of the core sections indicate that core recovery was very high, with only minimal gaps. We assumed that the top of the recovered core corresponds to the top of the drilled interval. Samples are stored in the collection of the Department of Earth Sciences of Utrecht University.

2.2. Lithostratigraphic units

We provide an overview of the lithostratigraphic formations in chronological order and their tentative ages based on earlier work (*e.g.*, Thomas, 1949; Otero *et al.*, 2012; Malumián *et al.*, 2013). Table 2 presents a summary and reference to the localities (Fig. 1) where we sampled these formations.
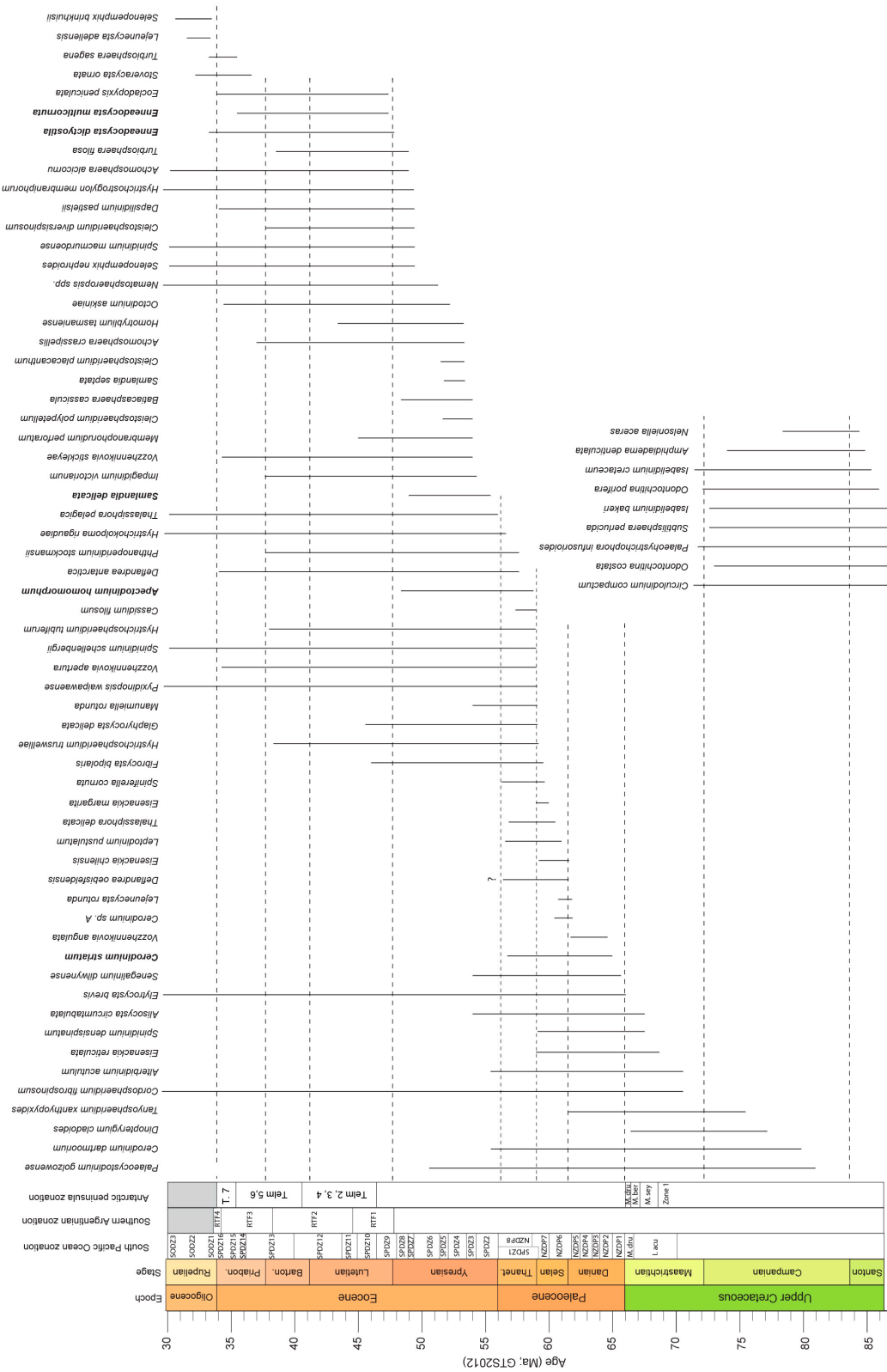
FIG. 2. Epochs, stages and published Southern Hemisphere dinoflagellate cyst zonations from the Southwest Pacific Ocean (Bijl *et al.*, 2013b, 2018; Crouch *et al.*, 2014; Houben *et al.*, 2019), Southern Argentina (González Estebenet *et al.*, 2016), and Antarctic Peninsula (Askin, 1988; Douglas *et al.*, 2014), and the published stratigraphic ranges (see also Table 3) of those dinoflagellate cyst species that are relevant for this study. The bioevents of the species names in bold serve as formal zone boundary definitions in dinoflagellate cyst zones of Bijl *et al.* (2013b) and Crouch *et al.* (2014). Dashed horizontal lines indicate stage boundaries.

TABLE 1. GEOGRAPHIC LOCATION OF OUTCROPS AND CORES, WITH FORMATION NAMES AND TENTATIVE AGE.

Outcrop/core	# of samples analysed for palynology	Region	Formation	Age	Latitude	Longitude
Río Pérez Outcrop	19	Laguna Blanca	Chorrillo Chico	Paleocene	52°32'1.56" S	72° 6'22.41" W
T-1 Well	9	Laguna Blanca	Leña Dura and Loreto	middle Eocene	51°46'18.55" S	72°18'52.30" W
Río Los Palos outcrop	10	Isla Riesco	Loreto	late Eocene	52°42'3.66" S	71°45'31.34" W
SELK-65 Well	15	Isla Riesco	Leña Dura	middle Eocene	52°42'24.20" S	71°48'51.71" W
Pecket Mine outcrop	8	Brunswick Peninsula	Loreto	late Eocene-Oligocene?	52°57'32.96" S	71° 9'34.04" W
RGP-03 Well	29	Brunswick Peninsula	Tres Brazos	early Eocene	53°3'57.98" S	71°16'7.20" W
Fuentes outcrop	2	Laguna Blanca	Fuentes	early Campanian	52°32'34.26" S	72° 1'26.77" W
IR-CAPO outcrop	3	Isla Riesco	Rocallosa	Maastrichtian	52°38'51.01" S	71°58'4.39" W
IR-CC outcrop	5	Isla Riesco	Chorrillo Chico	Paleocene	52°40'24.71" S	71°57'9.62" W
IR-AGFR outcrop	2	Isla Riesco	Agua Fresca	Paleocene-Eocene	52°40'35.98" S	71°56'57.27" W
IR-3B outcrop	2	Isla Riesco	Tres Brazos	early Eocene	52°41'30.95" S	71°53'47.61" W

2.2.1. Fuentes Formation

The Fuentes Formation (Hoffstetter *et al.*, 1957; Thomas, 1949) is a thick (up to 1,200 m) succession of platform sediments including shales, glauconitic sandstones with ripples marks and cross-bedding. According to Charrier and Lahsen (1969), García (1952) raised the unit to Formation rank, and distinguished a lower shale, a middle sandstone, and an upper shale. The Fuentes Formation reflects voluminous sediment supply from the Andean orogeny (Charrier and Lahsen, 1969). Published age for the Fuentes Formation is early Maastrichtian (Malumián *et al.*, 2013). The contact with the overlying formation has been a matter of debate: while Thomas (1949) suggested it was clearly non-conformable, Charrier and Lahsen (1969) put this into question. Both studies agree on a sharp lithological transition between both formations.

2.2.2. Rocallosa Formation

The Rocallosa Formation (Hoffstetter *et al.*, 1957) raised by Thomas (1949) to the rank of Formation, consists of hard, conglomeritic and coarse sandstone wedges, alternated with intervals of fine shales and siltstones (Charrier *et al.*, 2007). The sediment in the Rocallosa Formation is gradually fining upwards. Zircon dating suggests a late Maastrichtian age (67 Ma; Malumián *et al.*, 2013). A hiatus has been suggested between the Rocallosa and the overlying Chorillo Chico Formation (Malumián *et al.*, 2013).

2.2.3. Chorrillo Chico Formation

The Chorrillo Chico Formation (Thomas, 1949) consists of compact, brown indurated claystone, sporadically intercalated with (occasionally glauconitic) sandstone lenses and concretions (Otero *et al.*, 2012). Dinoflagellate cyst biostratigraphy and zircon dating suggest a Thanetian age (58-56 Ma; Quattrocchio, 2009; Malumián *et al.*, 2013).

2.2.4. Agua Fresca Formation

The Agua Fresca Formation (Hoffstetter *et al.*, 1957) is locally up to 2,000 m thick, and consists of microfossil-rich light grey mudstones and sandstones (Otero *et al.*, 2012), with concretions and

TABLE 2. LITHOSTRATIGRAPHIC FORMATIONS IN CHILEAN SOUTHERN PATAGONIA.

Formation	Lithology	Tentative age (*)	Present in							
			Río Pérez	Fuentes	T-1, T-22	IR	SELK-65	Río Los Palos	RGP-03	Pecket
Loreto	Thick cross-bedded sandstone units, heterolithic beds, concretions and coal	late Eocene	-	-	-	-	-	X	-	X
Leña Dura	Grey shales with marine macro and micro-invertebrates	middle Eocene	-	-	X	X	X	-	-	-
Tres Brazos	Silt-sandstones with conglomerate lenses and coal	early Eocene	-	-	-	X	-	-	X	-
Aqua Fresca	Microfossil-rich claystones and sandstones	early Eocene	-	-	-	X	-	-	-	-
Chorillo Chico	Dark grey claystones, alternating with green siltstones. sand lenses and concretions	Paleocene	X	-	-	X	-	-	-	-
Rocallosa	Hard conglomeritic sands-tones alternating with minor heterolithic shales	Late Cretaceous	X	-	-	X	-	-	-	-
Fuentes	Alternating dark grey-dark green shales	Late Cretaceous	-	X	-	-	-	-	-	-

(*) Their tentative age according to the literature (for reference see text), and the localities (see Fig. 1) where these formations were sampled.

minor glauconite horizons (Malumián *et al.*, 2013). Foraminifer stratigraphy indicates an early Eocene age (56-48 Ma; Malumián *et al.*, 2013). A 3 Myr hiatus has been suggested between the Agua Fresca and Tres Brazos formations (Malumián *et al.*, 2013).

2.2.5. Tres Brazos Formation

The Tres Brazos Formation represents eastward prograding delta deposits consisting of glauconitic silt- and sandstones, intercalated with conglomerate lenses and coal seams (Charrier *et al.*, 2007). In some studies (*e.g.*, Otero *et al.*, 2012; Malumián *et al.*, 2013) the Tres Brazos Formation and the Leña Dura Formation are considered one single formation. Age is tentatively mid-Eocene (Malumián *et al.*, 2013).

2.2.6. Leña Dura Formation

According to Otero *et al.* (2012), the Leña Dura Formation (Natland *et al.*, 1974) consists of grey, hard shales, which are rich in marine invertebrate and microfossils, particularly within concretions. Pioneering dinoflagellate cyst stratigraphy by Cookson and Cranwell (1967) suggested a late Eocene age for

the formation, which was later adjusted to middle Eocene by Malumián *et al.* (2013).

2.2.7. Loreto Formation

The Loreto Formation (Hoffstetter *et al.*, 1957) was deposited in shallow-marine to terrestrial environments based on the abundance of macrofossils (bivalves, gastropods and vertebrates; Otero *et al.*, 2012) and, increasingly upwards, coal seams (Thomas, 1949). The lithology consists of well-sorted sandstones, heterolithic beds, concretionary horizons. Several coal seams (Otero *et al.*, 2012) indicate an occasional terrestrial depositional environment for the unit. This formation is tentatively dated to be late Eocene (Otero *et al.*, 2012).

2.3. Laguna Blanca region: sections and samples

2.3.1. Río Pérez; Chorrillo Chico Formation

The outcrop is located on the east coastal cliff of a southward extending peninsula into the Otway Sound (Fig. 1C). We sampled the Chorrillo Chico Formation starting directly above the Rocallosa

Formation stratigraphically up-section, from S to N. Strata dip about 30° NW (Fig. 3). The section is comparatively well exposed, particularly in the storm flood level area. The top of the Chorrillo Chico Formation was not recognized; vegetation overgrowth obscures the sediment exposure towards the top of the section (Fig. 3). Sediments consist of relatively soft shales, alternating grey, green grey and light brown, with occasional harder, sandier levels (Figs. 3, 4).

2.3.2. Fuentes; Fuentes Formation

The top of the Fuentes Formation was sampled at a road construction site of road Y-50. Fresh material was collected from a recently blasted outcrop showing vertically dipping, roughly N-S striking 0.5-1 m thick alternations of greenish grey and dark grey siltstones. The road cut also revealed the boundary between the Fuentes and overlying Rocallosa Formations, which appears very sharp at this location.

2.3.3. Wells T-1 and T-22; Leña Dura and Loreto formations

Well T-1 was drilled in the northern part of the Laguna Blanca region in Chile, near the Argentinian border and Puerto Natales (Fig. 1C). The sedimentary rocks correspond to part of the Leña Dura Formation. The sequence consists of siltstone shales, interrupted by two thick sandstone units with conglomerates at the base (Fig. 5). The top part of the recovered sequence

contains an 8 m thick coal layer. We therefore infer that T-1 and T-22 recovered the boundary between the Leña Dura and Loreto formations. A ~10 kg sample for zircon radiometric dating was obtained from a core in the T-22 well (not shown), ~250 m NE of T-1. The sample corresponds to a medium to coarse-grain sandstone, located just above the same thick coal seam as was recovered at well T-1 (Fig. 5). We sampled cores 1-21 of T-1 at a resolution of 150 cm.

2.4. Isla Riesco region: sections and samples

2.4.1. North-coastal outcrops Isla Riesco; Rocallosa, Chorrillo Chico, Agua Fresca, Tres Brazos formations

We followed road Y-50 along the north shore of eastern Isla Riesco. The shore features outcrops of Eocene sediments, which are close to horizontal, with some gentle E-W compressional folding (Fig. 1C, D). As a result of this, and because of the abundance of vegetation overgrowth, the stratigraphic thickness of the Eocene deposits is difficult to establish with precision and therefore the stratigraphic height of the samples (Supplement 1) should be considered a rough estimate. The few outcrops along this shore consisted of <1 m high storm wave-induced cliff faces where we were able to sample exposures corresponding to the Rocallosa (CAPO), Chorrillo Chico (CC), Agua Fresca (AGFR), Tres Brazos (3B)

FIG. 3. Photograph showing part of the Chorrillo Chico Formation, at the sampled Río Pérez section, Laguna Blanca region, Chile (see Fig. 1 for locality). Image was taken towards the west. Horizontal scale: section approx. 200 m. The position of samples used in this study are indicated above the white line, number below the white line indicate stratigraphic height (m) above thick sandstone.
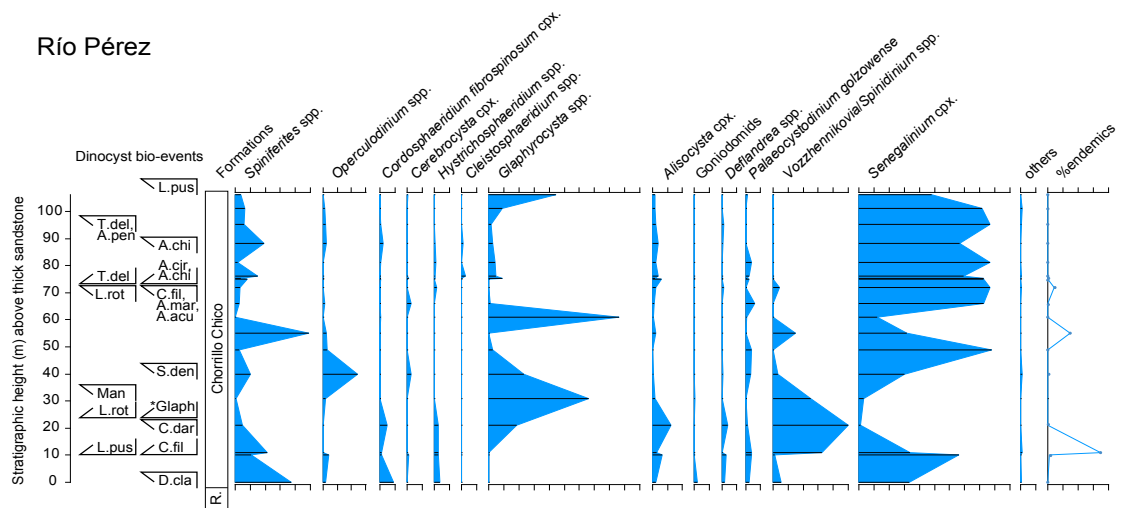
FIG. 4. Results from the Río Pérez section. Dinoflagellate cyst bioevents: **L.pus:** Leptodinium pustulatum, **D.cla:** Dinopterygium cladoides, **C.fil:** Cassidium filosum, **C.dar:** Cerodinium dartmooori, **Man:** Manumiella spp., ***Glaph:** acme of Glaphyrocysta spp., **L.rot:** Lejeunecysta rotunda, **S.den:** Spinidinium densispinatum, **A.acu:** Alterbidinium acutulum, **A.mar:** Alisocysta margarita, **A.cir:** Alisocysta circumtabulata, **A.chi:** Alisocysta chilensis, **T.del:** Thalassiphora delicata, **A.pen:** Alterbidinium pentaradiatum. Dinoflagellate cyst events that are above or below the presented section define minimum or maximum ages for the section, respectively. Formations (**R.:** Rocallosa Formation). Dinoflagellate cyst assemblages (in relative abundances of the in situ dinoflagellate cyst assemblage) plotted as eco-groups (following Sluijs *et al*., 2005) from the Río Pérez section (horizontal axis tick unit is 10%). Dinoflagellate cyst eco-groups are ordered from distal to coastal gonyaulacoid cysts, and then peridinioid cysts. Also plotted are % endemic dinoflagellate cysts. For raw counts see supplementary material. For which species are considered endemics see Methods.

formations (Supplement 1). Unfortunately, the formation boundaries could not be seen in the field, due to abundance of overgrowth and lack of exposed rocks. At this location, the Rocallosa Formation consists of thick, consolidated, reddish-brown medium-sandstones, intercalated with fine-grained siltstones with clay. The transition to Chorrillo Chico Formation is reflected by the disappearance of the sandstone layers; the sediments grade into silt-sized, homogeneous shales. The Agua Fresca Formation was recognized in the field as a 2 m thick conglomerate, followed by 6 m of unexposed section, 6 m of dark grey shales and 2 m of green sands. Sediments of Tres Brazos Formation consist of dark brown shales, with abundant root mottling.

2.4.2. Well SELK-65; Leña Dura Formation

Well SELK-65 was drilled west of the Río Los Palos section (Fig. 1D), and sediments include part of the Leña Dura Formation. The sediments are fine-grained siltstones, dark, but the cores are relatively intensely shattered (Fig. 6). We sampled Cores 1-15 at a resolution of 50 cm. Cores 4-6 were missing.

2.4.3. Río Los Palos; Loreto Formation

The Río Los Palos valley reaches the Otway Sound (Fig. 1D) at Estancia San Carlos. The valley allows sampling the upper Eocene Loreto Formation. Outcrops are well-accessible on either side of the valley, and consist of extensive marine and fluvial facies, that included fine-grained heterolithic sediments at the base. Leaf debris is abundant throughout the section, but one 5 m thick finer-grained sediment unit contained marine macrofossil remains (Fig. 7). Paleo-current orientation based on sediment structures is consistently from the east (NE to SE). We sampled relatively fine grained sediments at several stratigraphically successive outcrops exposed along the river, up to approximately 3 km upstream from the Estancia.

2.5. Brunswick Peninsula region: sections and samples

2.5.1. Well RGP-03; Tres Brazos Formation

Well RGP-03 was drilled approximately 15 km southwest of the Pecket Mine (Fig. 1C), and recovered
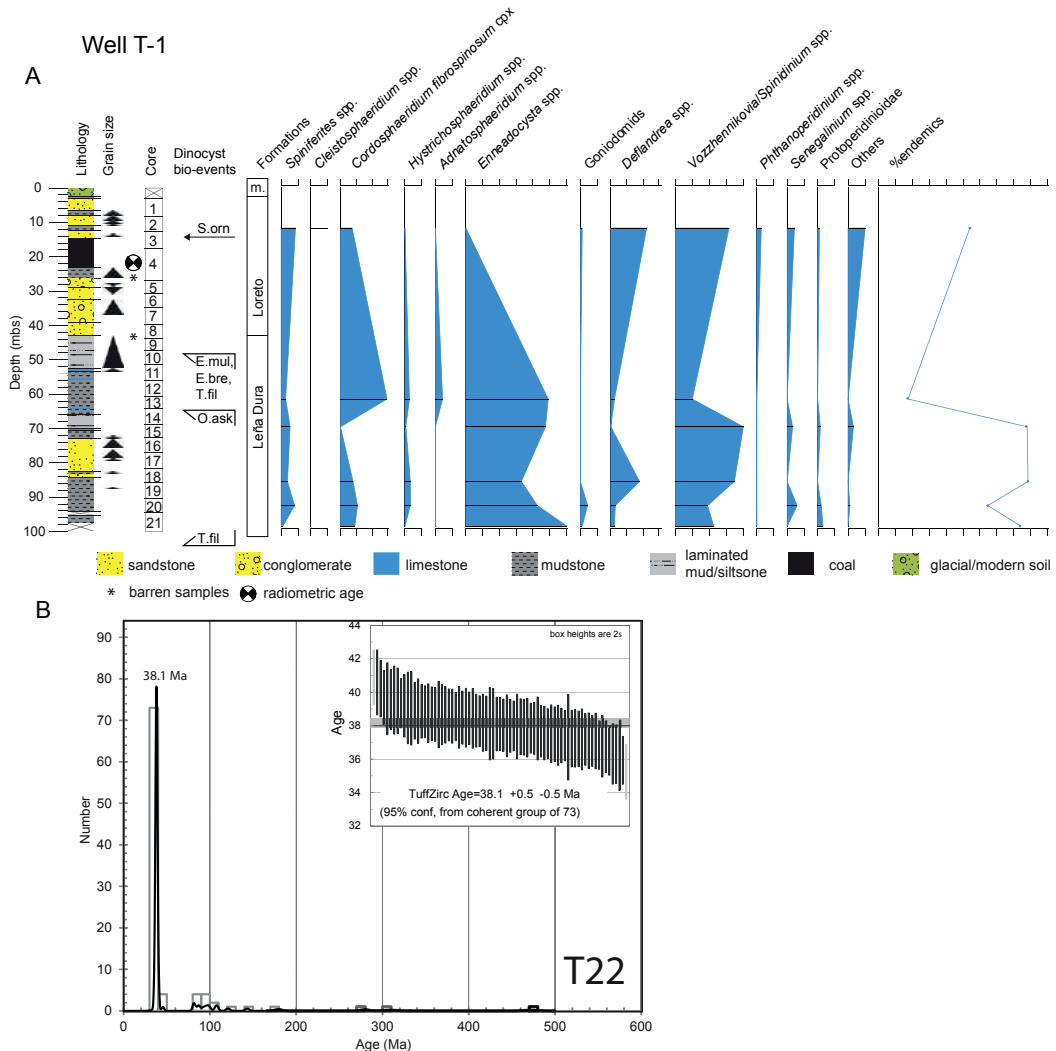
FIG. 5. **A.** Results from well T-1. Core description and legend, core sections. Black triangles indicate fining upward sequences. Dinoflagellate cyst bioevents: **T.fil:** Turbiosphaera filosa, **O.ask:** Octodinium askiniae, **E.mul:** Enneadocysta multicornuta, **E.bre:** Enneadocysta brevistila, **S.orn:** Stoveracysta ornata. Formations (**m.:** modern soil). Dinoflagellate cyst events that are above or below the presented section define minimum or maximum ages for the section, respectively. Dinoflagellate cyst eco-groups and relative abundance of endemic dinoflagellate cysts (horizontal axis tick unit is 10%). For core location see figure 1. Dinoflagellate cyst eco-groups are ordered from distal to coastal gonyaulacoid cysts, and then peridinioid cysts. **B.** Results of zircon U-Pb ages from well T-22. The stratigraphic location of the sample taken for zircon analyses in T-22 could be well-correlated to the nearby T-1 well and is indicates at ~21 m. Seventy-four out of 93 zircons were grouped in a major peak at 38.1±0.5 Ma, with a unimodal distribution.

part of the lower/middle Eocene Tres Brazos Formation. Sediments consist of consolidated, light-colored alternation of massive sandstones and wavy laminated heterolithic units (Fig. 8). Sandstone units become coarser up-section.We sampled Cores 2-25 at a resolution of 80 cm. Core 18 features a 30 cm thick oyster bed.

2.5.2. Pecket Mine; Loreto Formation

The open mine pit Pecket on the west coast of northern Brunswick Peninsula (Fig. 1C) reaches a depth of 120 m into the subsurface (Fig. 9). The section consists of an alternation of siltstone shales, incisive, fining upwards sandstone channels, heterolithic units and coal deposits. Fossil leaf
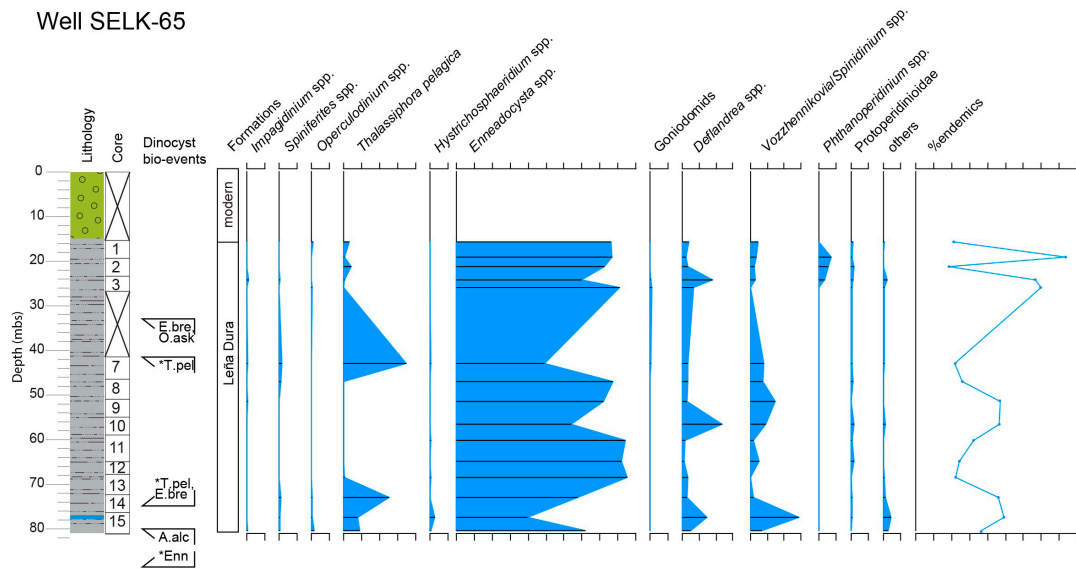
FIG. 6. Results from well SELK-65. Core description (for legend see Fig. 5), core sections. Dinoflagellate cyst bioevents: ***Enn:** acme Enneadocysta spp., **A.alc:** Achomosphaera alcicornu, ***T.pel:** acme Thalassiphora pelagica, **O.ask:** Octodinium askiniae, **E.bre:** Enneadocysta brevistila. Dinoflagellate cyst events that are above or below the presented section define minimum or maximum ages for the section, respectively. Dinoflagellate cyst eco-groups and relative abundance of endemic dinoflagellate cysts (horizontal axis tick unit is 10%). For core location see figure 1. Dinoflagellate cyst eco-groups are ordered from distal to coastal gonyaulacoid cysts, and then peridinioid cysts.

debris and bioturbation are common throughout the section, which covers part of the Loreto Formation. One ~10 kg sample was taken from the base of the section for U/Pb radiometric dating of zircons from a white volcanic ash located inside coals (Tonstein; Fig. 9).

3. Methods

3.1. Palynology

The palynological processing techniques applied to a selection of 104 samples from the various locations (Table 1) were previously described by Bijl *et al.* (2013a). Briefly, this involves freeze-drying, crushing of the sediment to millimeter-size chips and spiking of the sample with a known amount (9,666 specimens +/- error per sample) of *Lycopodium clavatum* spores, to enable quantitative assessment of dinoflagellate cysts. Chemical treatment included two rounds of (38%) HF digestion, followed by (30%) HCl rinsing steps to eliminate the fluoride gels that emerged from silicate digestion. Kerogen residues we subsequently sieved, with help of an

ultrasonic bath to break up clumps of amorphous organic matter. The 250 to 10 µm size fraction was mounted on microscope slides for analyses of palynomorphs. The minimum count completed was 200 specimens where possible: for some samples, yields were too low to achieve this. We discarded samples with counts below 30. Taxonomy follows that cited in Williams *et al.* (2017) except for the subfamily Wetzellioideae, for which we follow recommendations in (Bijl *et al.*, 2016). Dinoflagellate cyst counting was performed under light microscopy with 400x magnification. Palynological residues and slides were stored in the collection of the Marine Palynology and Paleoceanography group, Laboratory of Palaeobotany and Palynology, Department of Earth Sciences, Utrecht University.

3.2. Stratigraphy

Assessment of the calibration of dinoflagellate cyst bioevents follows that in the available literature. Helby *et al.* (1987) calibrated dinoflagellate cyst bioevents from Australia to Cretaceous ammonite zonations. Mao and Mohr (1992) recognized dinoflagellate cyst
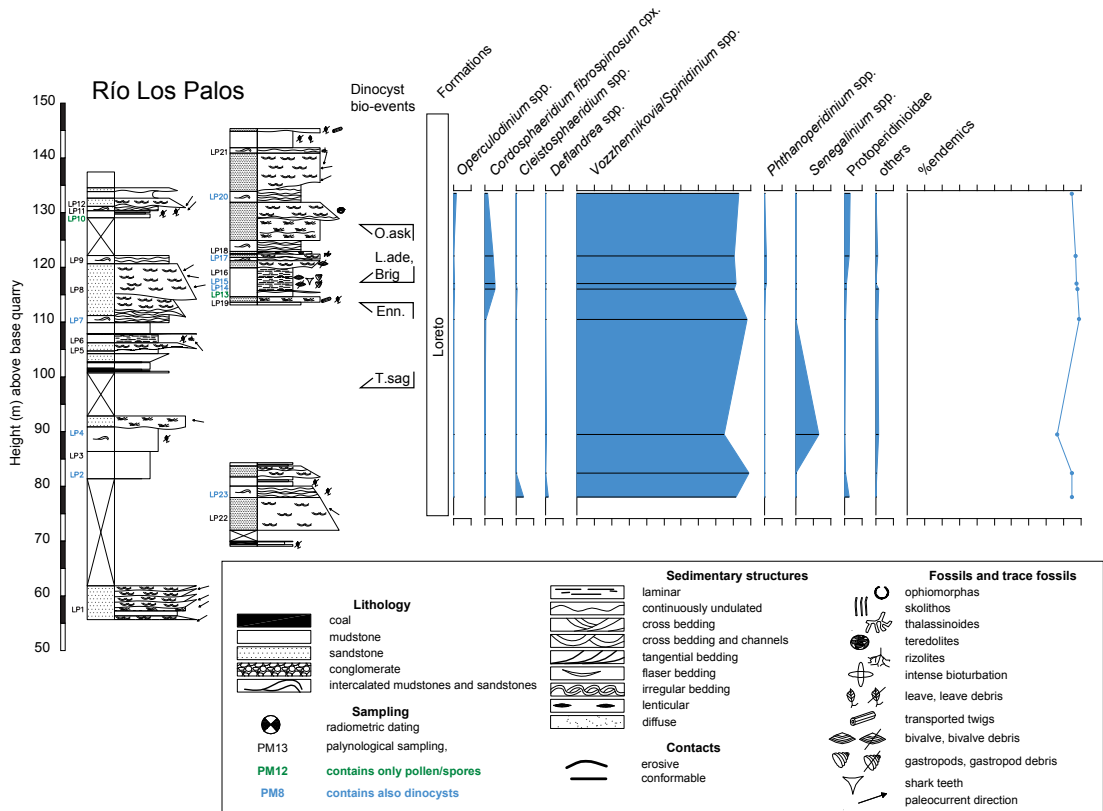
FIG. 7. Results from Río Los Palos. Lithologic log of outcrops along the river valley (see section 2.4.3), sample positions. Dinoflagellate cyst bioevents: **T.sag:** Turbiosphaera sagena, **Enn.:** Enneadocysta spp., **Brig.:** Brigantedinium spp., **L.ade:** Lejeunecysta adeliense, **O.ask:** Octodinium askiniae. Dinoflagellate cyst eco-groups and relative abundance of endemic dinoflagellate cysts (horizontal axis tick unit is 10%). For location of the outcrops see figure 1. Dinoflagellate cyst eco-groups are ordered from distal to coastal gonyaulacoid cysts, and then peridinioid cysts.

bioevents in sediments from Maud Rise, which were independently dated using nannofossil stratigraphy. Frieling *et al.* (2018) identified dinoflagellate cyst bioevents from the Paleocene-Eocene Boundary interval in South Australia, calibrated using stable carbon isotope stratigraphy. Sluijs *et al.* (2003) calibrated dinoflagellate cyst bioevents from late Eocene-Oligocene successions around Tasmania to the available magnetostratigraphy, which in turn was interpreted using diatom, nannofossil and foraminifer biostratigraphy. This study was later expanded, updated and refined by Houben *et al.* (2019). Bijl *et al.* (2013b) updated and expanded the work by Brinkhuis *et al.* (2003b) on dinoflagellate cyst bioevents from Maastrichtian-Eocene sediments from offshore Tasmania. Using additional independent constraints from isotope stratigraphy and recalibrating the ages to the

GTS2012 time scale of Gradstein *et al.* (2012), Bijl *et al.* (2013b) provided a dinoflagellate cyst zonation scheme. This scheme could also be tied to Paleocene-Eocene zonations for New Zealand (Crouch and Brinkhuis, 2005; Crouch *et al.*, 2014). We also compare our dinoflagellate cyst bioevents to those presented in zonations from Southern Argentina (González Estebenet *et al.*, 2016), which consistently follow that of the southwest Pacific Ocean, and benefit from radiometric dating. We plot the known stratigraphic ranges of dinoflagellate cyst species in figure 2 and provide the ages of the bioevents in table 3.

3.3. Assessing dinoflagellate cyst endemism

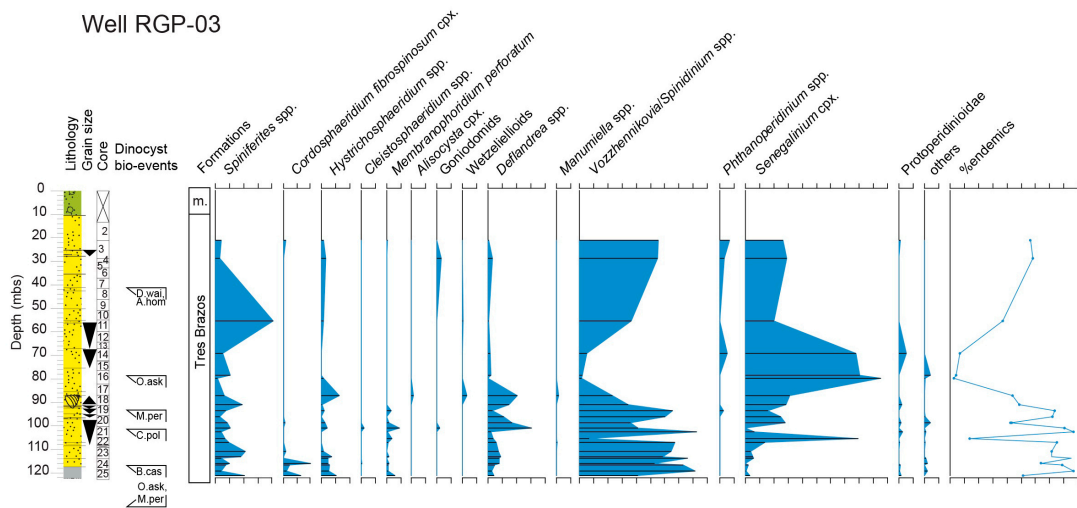Assignment of biogeographic affinities of dinoflagellate cysts follow that in Bijl *et al.* (2011),

FIG. 8. Results from well RGP-03. Core description (for legend see Fig. 5), cores. Dinoflagellate cyst bioevents: **B.cas:** Batiacasphaera cassicula, **C.pol:** Cleistosphaeridium polypetellum, **M.per:** Membranophoridium perforatum, **O.ask:** Octodinium askiniae, **D.wai:** Dracodinium waipawaense, **A.hom:** Apectodinium homomorphum. Dinoflagellate cyst events that are above or below the presented section define minimum or maximum ages for the section, respectively. Lithology (**m.:** modern). Dinoflagellate cyst eco-groups and relative abundance of endemic dinoflagellate cysts. Samples with counts below 30 were discarded from the assemblage plot. For core location see figure 1. Dinoflagellate cyst eco-groups are ordered from distal to coastal gonyaulacoid cysts, and then peridinioid cysts (horizontal axis tick unit is 10%).

with modifications proposed by Sluijs and Brinkhuis (2009), Frieling and Sluijs (2018) and Cramwinckel *et al*. (2019) on the non-endemic nature of *Phthanoperidinium stockmansii* and *Hystrichosphaeridium truswelliae*. The endemic dinoflagellate cysts are those that are biogeographically restricted to the Southern Ocean or are bi-polar. The other taxa are hence cosmopolitan (*e.g.*, *Spiniferites*, *Glaphyrocysta*, *Cordosphaeridium*, *Cleistosphaeridium*, *Senegalinium*) but we might also encounter species with clear affinities to warmer temperatures and lower latitudes (*e.g.*, the Wetzelielloids or Goniodomideae; Frieling *et al*., 2014; Frieling and Sluijs, 2018).

3.4. Paleoceanographic interpretation dinoflagellate cyst assemblages

Following earlier work (see *e.g.*, Sluijs *et al.*, 2005 for an overview) the dinoflagellate cyst assemblages are presented in eco-groups, according to their preferred niche on the continental shelf. This grouping allows qualitative detection of changes in paleoceanographic conditions: distance to shore, surface-water nutrient conditions, surface-water

salinity and runoff and allows identification of transgressive sands. Recently, these qualitative ecologic affinities were semi-quantitatively constrained by Frieling and Sluijs (2018). Table 4 provides the ecologic affinities of dinoflagellate cyst eco-groups.

3.5. U-Pb dating of detrital zircons

Zircons in this study were analyzed for their U-Pb age at the Radiogenic Isotope and Geochronology Lab (RIGL) at Washington State University. We use the data reduction protocol described in detail by Chang *et al*. (2006), which we also briefly discuss here. Each analysis consists of a 30 second gas blank followed 30 seconds of ablation. Analyses were conducted using a New Wave 213 nm solid state (Nd:YAG) laser ablation system couple to a ThermoFinnigan Element2 ICPMS. Laser ablation parameters used for this study employed laser spot size diameters of 30 μm, with a repetition rate of 10Hz, and a few of ~4-5 J/cm^2. For each analysis, the first ~6 seconds of data produced, as the sample signal reaches maximum signal intensity, are not considered. The next ~30 seconds of data are used to calculate U-Th-Pb isotope ratios by measuring the intensities
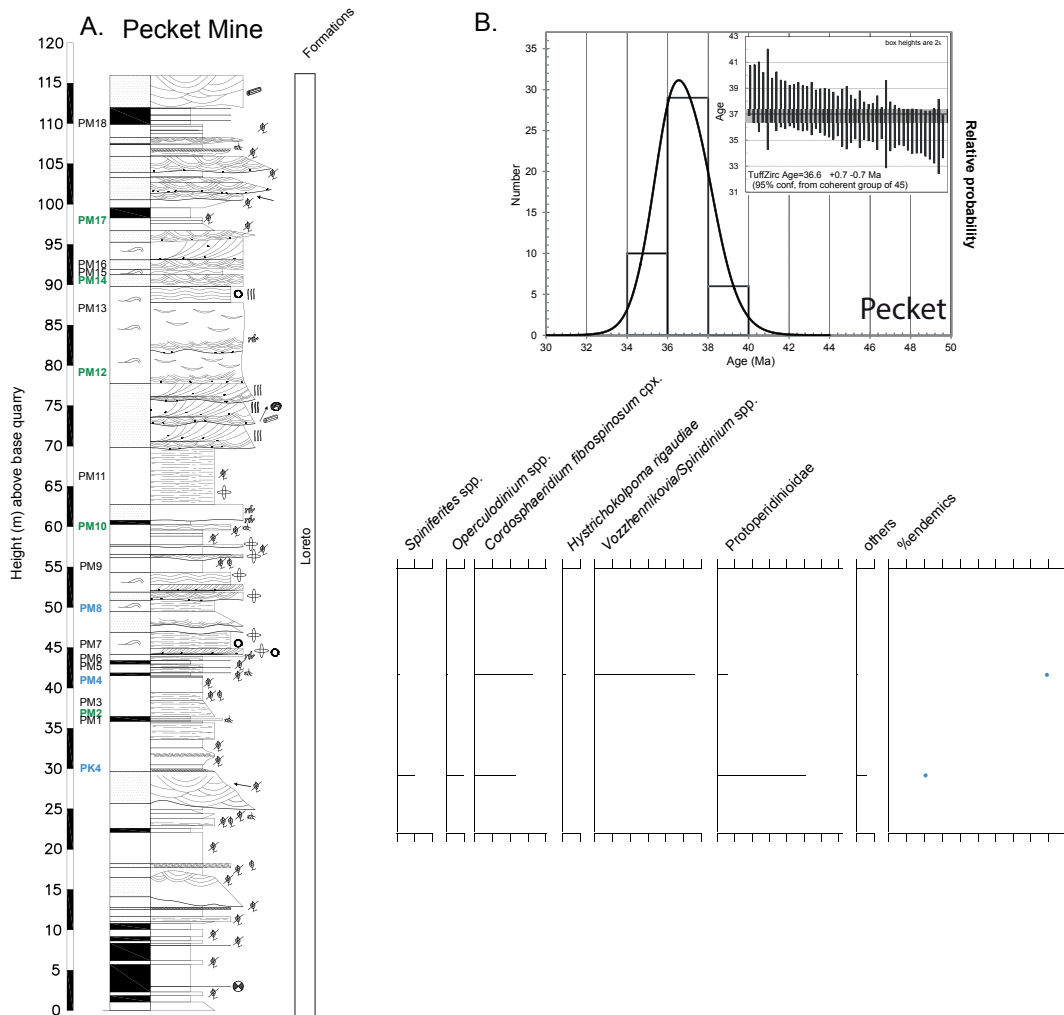
FIG. 9. **A.** Results from the Pecket Mine outcrop. Lithologic log (for legend see Fig. 7), sample positions and dinoflagellate cyst eco-groups and relative abundance of endemic dinoflagellate cysts. For core location see figure 1. Dinoflagellate cyst eco-groups are ordered from distal to coastal gonyaulacoid cysts, and then peridinioid cysts (horizontal axis tick unit is 10%). **B.** Results of zircon U-Pb radiometric dates, where 45 zircons were analyzed with a primary uni-modal distribution yield an age of 36.6±0.7 Ma.

at masses ^{202}Hg, ^{204}Pb+Hg, ^{206}Pb, ^{207}Pb, ^{208}Pb, ^{232}Th, ^{235}U and ^{238}U during ~300 sweeps through the mass range. The mean count rate of each isotope during the 30-second gas blank (300 sweeps) is subtracted from each sweep through the mass range collected during ablation (300 sweeps). Following gas blank (*i.e.*, "background") correction, ^{206}Pb/^{238}U, ^{207}Pb/^{235}U, and ^{207}Pb/^{206}Pb ratios are determined for each sweep for both samples and standards. Due to the well-known phenomenon of U-Pb elemental fractionation during laser ablation, which manifests as increasing U-Pb ratios

with ablation depth (*e.g.*, Jackson *et al.*, 2004; Paton *et al.*, 2010), we account for variable U-Pb fractionation, using the intercept method of Sylvester and Ghaderi (1997) for the U-Pb ratios. Conversely, the measured ^{207}Pb/^{206}Pb is determined using the arithmetic mean of all sweeps, as there is no observable fractionation of this ratio as ablation proceeds.

Analyses of unknown zircons and quality control zircons are interspersed with analyses of external calibration standards, typically with 7-10 unknowns bracketed by multiple analyses of two different zircon

TABLE 3. DINOFLAGELLATE CYST BIOEVENTS AND ECOLOGIC AND BIOGEOGRAPHIC AFFINITY. (*)

Species	FAD	LAD	Source	Region	P or G	Eco-group	Endemic?
Achomosphaera alcicornu	48.9	-	Bijl *et al.*, 2013b	Australia	G	*Spiniferites* cpx	No
Achomosphaera crassipellis	53.3	37.0	Bijl *et al.*, 2013b	Australia	G	*Spiniferites* cpx	No
Adnatosphaeridium sp.	-	-	-	-	G	*Adnatosphaeridium* spp.	No
Alisocysta circumtabulata	67.5	54.0	Helby *et al.*, 1987; Bijl *et al.*, 2013b	Australia	G	*Alisocysta* cpx	No
Alisocysta margarita	60.0	59.0	Crouch *et al.*, 2014	New Zealand	G	*Alisocysta* cpx	No
Alterbidinium acutulum	70.6	55.5	Mao and Mohr, 1995; Raine *et al.*, 1997	Kerguelen *Plateau*; Australia	P	*Senegalinium* cpx	No
Alterbidinium pentaradiatum	64.4	61.9	Crouch *et al.*, 2014	New Zealand	P	*Senegalinium* cpx	No
Amphidiadema denticulata	85	74	Helby *et al.*, 1987; Mohr and Mao, 1997	Australia; Kerguelen *Plateau*	P	*Senegalinium* cpx	No
Apectodinium homomorphum	58.8	48.3	Bijl *et al.*, 2013b	Australia	P	*Wetzeliellioidae*	No
Areoligera sp.	-	-	-	-	G	*Glaphyrocysta* cpx	No
Batiacasphaera cassicula	54.0	48.3	Bijl *et al.*, 2013b	Australia	G	*Alisocysta* cpx	No
Brigantedinium simplex	40.0	0.0	Bijl *et al.*, 2013b	Australia	P	Protoperidinioidae	No
Cassidium filosum	59.0	57.3	Bijl *et al.*, 2013b	Australia	G	*Alisocysta* cpx	No
Cassidium fragile	65.7	34.4	Raine *et al.*, 1997; van Mourik *et al.*, 2001	Australia; N atlantic	G	*Alisocysta* cpx	No
Cerebrocysta bartonensis	53.7	38.6	Brown and Downie, 1984; Powell, 1992	North Sea	G	*Cerebrocysta* cpx	No
Cerodinium dartmoorium	-	55.4	Bujak and Mudge, 1994	North Sea	P	*Deflandrea* cpx	No
Cerodinium sp. A small s*ensu* 1172	61.9	59.9	Bijl, personal observation, 2020	Australia	P	*Deflandrea* cpx	No
Cerodinium striatum	67.0	56.8	Brinkhuis *et al.*, 2003b; Bijl, personal observation, 2020	Australia	P	*Deflandrea* cpx	No
Circulodinium distinctum	-	-	-	-	G	*Glaphyrocysta* cpx	No
Cleistosphaeridium diversispinosum	49.3	37.8	Bijl *et al.*, 2013b	Australia	G	*Cleistosphaeridium* spp.	No
Cleistosphaeridium placacanthum	53.3	51.4	Bijl *et al.*, 2013b	Australia	G	*Cleistosphaeridium* spp.	No
Cleistosphaeridium polypetellum	54.0	51.6	Bijl *et al.*, 2013b	Australia	G	*Cleistosphaeridium* spp.	No
Cordosphaeridium fibrospinosum	70.5	31.6	Williams *et al.*, 1993	North Atlantic	G	*Cordosphaeridium fibrospinosum* cpx	No
Dapsilidinium pastielsii	37.1	37.4	van Mourik *et al.*, 2005	Eastcoast USA	G	*Diphyes* cpx	No
Deflandrea antarctica	57.7	-	Bijl *et al.*, 2013b	Australia	P	*Deflandrea* cpx	Yes
Deflandrea foveolata	62.4	58.7	Crouch *et al.*, 2014	New Zealand	P	*Deflandrea* cpx	No
Deflandrea oebisfeldensis	61.5	50.7	Raine *et al.*, 1997; Powell *et al.*, 1992	Southern Hemisphere; North Sea	P	*Deflandrea* cpx	No
Dinopterygium cladoides	-	66.4	Brinkhui*s et al.*, 2003b	Australia	G	Goniodomidae	No
Diphyes colligerum	61.5	31.5	Bijl *et al.*, 2013b; Brinkhuis and Biffi, 1993	Australia; North Sea	G	*Diphyes* cpx	No
Dracodinium waipawaense	54.0	50.0	Bijl *et al.*, 2013b	Australia	P	Wetzeliellioidae	No
Eisenackia chilensis	61.5	59.2	Bijl *et al.*, 2013b	Australia	G	*Alisocysta* cpx	No

Table 3 continued.

Species	FAD	LAD	Source	Region	P or G	Eco-group	Endemic?
Eisenackia reticulata	68.8	59.0	Brinkhuis *et al.*, 2003b; Crouch *et al.*, 2014	Australia; New Zealand	G	*Alisocysta* cpx	No
Elytrocysta brevis	65	53.9	Bijl, personal observation, 2020; Brown and Downie, 1984	C and N atlantic	G	*Elytrocysta* cpx	No
Enneadocysta brevistila	-	-	-	-	G	*Enneadocysta* spp.	Yes
Enneadocysta dictyostila	47.9	33.2	Bijl *et al.*, 2013b	Australia	G	*Enneadocysta* spp.	Yes
Enneadocysta multicornuta	47.3	35.3	Bijl *et al.*, 2013b	Australia	G	*Enneadocysta* spp.	No
Enneadocysta pectiniformis	42.8	26.9	Head and Norris, 1989; Egger *et al.,* 2016	N Atlantic	G	*Enneadocysta* spp.	No
Eocladopyxis peniculata	47.3	33.9	Bijl *et al.*, 2013b	Australia	G	Goniodomidae	Yes
Fibrocysta bipolaris	59.7	-	Masure *et al.*, 1998	C atlantic	G	*Cordosphaeridium fibrospinosum* cpx	No
Florentinia mantelli	131.4	65.7	Williams *et al.*, 1993; Eshet *et al.*, 1992	N Atlantic; Israel	G	*Diphyes* cpx	No
Glaphyrocysta delicata	59.1	45.7	Bijl *et al.*, 2013b	Australia	G	*Glaphyrocysta* cpx	No
Glaphyrocysta retiintexta	54.8	49.3	Bijl *et al.*, 2013b	Australia	G	*Glaphyrocysta* cpx	No
Glaphyrocysta semitecta	42.3	32.6	Firth, 1996; Pross *et al.*, 2012	N Atlantic; Italy	G	*Glaphyrocysta* cpx	No
Heteraulacacysta porosa	43.9	34.4	Gradstein *et al.*, 1992; Head and Norris, 1989	North Sea	G	Goniodomidae	No
Homotryblium tasmaniense	53.2	43.4	Bijl *et al.*, 2013b	Australia	G	Goniodomidae	No
Hystrichokolpoma rigaudiae	56.8	19.0	Crouch *et al.,* 2014	New Zealand	G	*Diphyes* cpx	No
Hystrichosphaeridium truswelliae	59.1	38.3	Bijl *et al.*, 2013b	Australia	G	*Hystrichosphaeridium* spp.	No
Hystrichosphaeridium tubiferum	59.0	38.0	Bijl *et al.*, 2013b	Australia	G	*Hystrichosphaeridium* spp.	No
Hystrichostrogylon membraniphorum	49.3	38.3	Bijl *et al.,* 2013b	Australia	G	*Spiniferites* cpx	No
Impagidinium dispertitum	-	-	-	-	G	*Impagidinium* spp.	No
Impagidinium maculatum	57.1	33.7	Raine *et al.*, 1997	Australia	G	*Impagidinium* spp.	No
Impagidinium victorianum	54.3	37.8	Bijl *et al.,* 2013b	Australia	G	*Impagidinium* spp.	No
Isabelidinium bakeri	76.8	71.7	Mao and Mohr, 1992; Mohr and Mao, 1997	Kerguelen *Plateau*	P	*Senegalinium* cpx	No
Isabellidinium cretaceum	85.2	71.7	Raine *et al.,* 1997	Australia	P	*Senegalinium* cpx	No
Kenleyia sp.	-	-	-	-	G	*Cordosphaeridium fibrospinosum* cpx	No
Lejeunecysta adeliense	33.7	32.6	Bijl *et al.*, 2018	Antarctica	P	Protoperidinioidae	No
Lejeunecysta hyalina	65.7	14.9	Eshet *et al.*, 1992; Zegarra and Helenes, 2011	Egypt; C America	P	Protoperidinioidae	No
Lejeunecysta rotunda (*sensu* 1172)	60.7	62.8	Bijl, personal observation, 2020	Australia	P	Protoperidinioidae	No
Leptodinium pustulatum	61.0	56.5	Crouch *et al.*, 2014	New Zealand	G	*Cerebrocysta* cpx	No
Lingulodinium machaerophorum	58.3	0.0	Bijl *et al.*, 2013b	Australia	G	Goniodomidae	No
Manumiella rotunda	59.1	53.2	Crouch *et al.*, 2014; Bijl *et al.*, 2013b	New Zealand; Australia	P	*Deflandrea* cpx	No
Manumiella seelandica	-	66.0	Bowman *et al.*, 2012	Antarctica	P	Deflandrea cpx	No
Manumiella? small	-	-	-	-	P	*Deflandrea* cpx	No

Table 3 continued.

Species	FAD	LAD	Source	Region	P or G	Eco-group	Endemic?
Membranophoridium perforatum	54.0	45.0	Bijl *et al*., 2013b	Australia	G	*Membranophoridium perforatum*	Yes
Microdinium sp.	-	-	-	-	G	*Elytrocysta* cpx	No
Muratodinium fimbriatum	58.6	50.6	Powell *et al*., 1992,1996	North Sea	G	*Glaphyrocysta* cpx	No
Nelsoniella aceras	84.3	78.4	Raine *et al*., 1997	Australia	P	*Deflandrea* cpx	No
Nematosphaeropsis sp.	51.4	-	Bijl *et al*., 2013b	Australia	G	*Nematosphaeropsis* spp.	No
Octodinium askiniae	52.2	34.5	Bijl *et al*., 2013b; Houben *et al*., 2019	Australia	P	other	Yes
Odontochitina costata	100	69.9	Tocher and Jarvis, 1996; Costa and Davey, 1992	Europe; North Sea	G	*Glaphyrocysta* cpx	No
Odontochitina porifera	89.9	70.1	Williams *et al*., 1993; Mao and Mohr, 1992	N Atlantic; Kerguelen *Plateau*	G	*Glaphyrocysta* cpx	No
Oligosphaeridium complex	137.7	48.8	Williams *et al*., 1993	N Atlantic	G	other	No
Operculodinium large sensu 1172	68.4	65.6	Brinkhuis *et al*., 2003b; Bijl, personal observation, 2020	Australia	G	*Operculodinium* spp.	No
Palaeocystodinium golzowense	81.0	50.7	Raine *et al*., 1997; Bijl *et al*., 2013b	Australia	P	*Palaeocystodinium* spp.	No
Palaeohystrichophora infusorioides	103	71.7	Helby *et al*., 1987	Australia	P	*Senegalinium cpx*	No
Phthanoperidinium stockmansii	57.7	37.8	Bijl *et al*., 2013b	Australia	P	*Phthanoperidinium* spp.	No
Protoperidinioideae	-	-	-	-	P	Protoperidinioids	No
Pyxidinopsis waipawaense	59.1	-	Bijl *et al*., 2013b	Australia	G	*Cerebrocysta* cpx	No
Rhombodinium draco	49.3	25.8	Bijl *et al*., 2013b; Sliwinska *et al*., 2012	Denmark	P	Wetzeliellioidae	No
Samlandia delicata	55.5	49.0	Bijl *et al*., 2013b	Australia	G	*Cordosphaeridium* fibrospinosum cpx	No
Samlandia septata	53.3	51.8	Bijl *et al*., 2013b	Australia	G	*Cordosphaeridium fibrospinosum* cpx	No
Selenopemphix brinkhuisii	33.4*	30.6	Bijl *et al*., 2018	Antarctica	P	Protoperidinioidae	No
Selenopemphix nephroides	49.3	-	Bijl *et al*., 2013b	Australia	P	Protoperidinioidae	No
Senegalinium dilwynense	65.7	54.0	Raine *et al*., 1997	Australia	P	*Senegalinium* cpx	No
Spinidinium densispinatum	65.7	-	Raine *et al*., 1997	Australia	P	*Vozzhennikovia* cpx	No
Spinidinium macmurdoense	56.8	30.0	Bijl *et al*., 2013b	Australia	P	*Vozzhennikovia* cpx	Yes
Spinidinium schellenbergii	59.0	-	Bijl *et al*., 2013b	Australia	P	*Vozzhennikovia* cpx	Yes
Spiniferella cornuta	59.7	56.2	Masure *et al*., 1998; Awad and Oboh-Ikenobe, 2016	C Atlantic	G	*Spiniferites* cpx	No
Stoveracysta ornata	36.7	30.8	Bijl *et al*., 2013b, 2018	Australia; Antarctica	G	*Alisocysta* cpx	No
Subtilisphaera perlucida	135.5	72.7	Leereveld, 1997; Mao and Mohr, 1992	Spain; Kerguelen *Plateau*	P	*Senegalinium* cpx	No
Tanyosphaeridium xanthiopyxides	75.2	61.6	Mao and Mohr, 1992; Masure *et al*., 1998	Kerguelen *Plateau*, C Atlantic	G	other	No
Tectatodinium pellitum	65.4	0.0	Powell, 1992	North Sea	G	*Cerebrocysta* cpx	No
Thalassiphora delicata	60.7	56.9	Brinkhuis *et al*., 2003b; Awad and Oboh-Ikenobe, 2016	Australia; C Atlantic	G	*Cordosphaeridium fibrospinosum* cpx	No

Table 3 continued.

Species	FAD	LAD	Source	Region	P or G	Eco-group	Endemic?
Thalassiphora pelagica	56.0	-	Bijl *et al.*, 2013b	Australia	G	*Cordosphaeridium fibrospinosum* cpx	No
Trithyrodinium vermiculatum	-	-	-	-	P	*Senegalinium* cpx	No
Turbiosphaera filosa	49.0	38.7	Bijl *et al.*, 2013b	Australia	G	*Cordosphaeridium fibrospinosum* cpx	No
Turbiosphaera sagena	35.7	33.2	Bijl *et al.*, 2013b	Australia	G	*Cordosphaeridium fibrospinosum* cpx	No
Vozzhennikovia angulata	64.7	61.9	Crouch *et al.*, 2014	New Zealand	P	*Vozzhennikovia* cpx	Yes
Vozzhennikovia apertura	59.0	34.1	Bijl *et al.*, 2013b; Houben *et al.*, 2019	Australia	P	*Vozzhennikovia* cpx	Yes
Vozzhennikovia roehliae	53.0	33.2	Bijl *et al.*, 2013b; Sluijs *et al.*, 2009	Australia	P	*Vozzhennikovia* cpx	Yes
Vozzhennikovia stickleyae	53.4	33.2	Bijl *et al.*, 2013b	Australia	P	*Vozzhennikovia* cpx	Yes

(*) Species name, first appearance data (**FAD**), last appearance data (**LAD**), source, region where these dinoflagellate cyst bioevents were calibrated (all (re-) calibrated to GTS2012 of Gradstein *et al.* (2012)) eco-group (see Table 4) and biogeographic affinity. **N:** North, **C:** Central, **P:** Peridinioid, **G:** Gonyaulacoid. This study suggests the FO might be older than the earliest Oligocene.

standards (Plešovice and FC-1). Plešovice (337 Ma; Sláma *et al.*, 2008) was used to calibrate the ^{206}Pb/^{238}U and ^{207}Pb/^{235}U ages, and FC-1 (1099 Ma; Paces and Miller, 1993) was used for calibration of ^{207}Pb/^{206}Pb, owing to much higher count rates for ^{207}Pb (~2-4 times higher than Plešovice). The concentrations of U, Th, Pb are estimated by interspersing analyses of NIST610 glass which has well characterized concentrations of these elements. Final ages were determined using a standard-sample bracketing approach. U-Pb zircon crystallization ages were estimated and plotted using Isoplot 3.0 (Ludwig, 2003).

4. Results

Raw counts of dinoflagellate cysts and the detailed results of U-Pb dating of zircons can be found in Supplement 1. A list of dinoflagellate cyst species encountered is presented in table 3 and selected specimens are illustrated in Plates 1 and 2. We here describe the dinoflagellate cyst biostratigraphy and assemblages per studied section and integrate these with the U-Pb dating results.

4.1. Laguna Blanca región

4.1.1. Río Pérez; Chorillo Chico Formation

All samples contain abundant, well-preserved, and diverse dinoflagellate cyst assemblages, as well as terrestrial palynomorphs. Stratigraphically important species include *Alisocysta circumtabulata*, *A. margarita*, *Eisenackia reticulata*, *E. chilensis*, *Alterbidinium pentaradiatum*, *Cassidium filosum*, *Cerodinium dartmoorium*, *C. striatum*, and a previously undescribed *Cerodinium* taxon termed *C. sp. A,* which was also observed in Paleocene strata at ODP Site 1172 on the East Tasman *Plateau* (P.K. Bijl, personal observation, 2020). We also recorded *Leptodinium pustulatum*, abundant *Glaphyrocysta*, *Isabelidinium bakeri*, *Lejeunecysta rotunda*, *Spinidinium densispinatum*, *Spiniferella cornuta*, *Tanyosphaeridium xanthiopyxides* and *Thalassiphora delicata* (Fig. 4). The lowermost sample contains few specimens of the typical Maastrichtian (Brinkhuis *et al.*, 1998, 2003b; Bowman *et al.*, 2012) dinoflagellate cyst markers *Manumiella seelandica* and *Dinopterygium cladoides*. The presence of *Leptodinim pustulatum* throughout, along with the remaining assemblage, and the absence of typical earliest Danian stratigraphic markers such as *Trithyrodinium evittii*, *Senoniasphaera inornata*, and *Palynodinium grallator*, as well as absence of *Palaeoperidinium pyrophorum* suggests that most of the Danian is missing from the sequence. The presence of *Alterbidinium pentaradiatum* in the top of the outcrop is the only species in disagreement with this inference because this species occurs in the lower Danian of New Zealand (Crouch *et al.*, 2014). A hiatus in the early Paleocene is consistent with

TABLE 4. ECOLOGIC AFFINITIES OF DINOFLAGELLATE CYST ECO-GROUPS.

Eco-group	Ecologic affinity	Source
Adnatosphaeridium	Mid-shelf	Sluijs *et al.*, 2005
Alisocysta	Unknown; high terrestrial input?	Frieling and Sluijs, 2018
Cerebrocysta	Outer neritic?	Prebble *et al.*, 2013
Cleistosphaeridium	Mid-shelf	Sluijs *et al.*, 2005
Cordosphaeridium fibrospinosum	Mid-shelf	Sluijs *et al.*, 2005
Deflandrea	High primary productivity, mid-shelf	Sluijs *et al.*, 2005
Diphyes colligerum	Lagoonal	Sluijs *et al.*, 2005
Elytrocysta	Mid-shelf?	Bijl, personal observation, 2020
Enneadocysta	Mid-shelf	Sluijs *et al.*, 2005
Glaphyrocysta	Mid-shelf, transgressive, dynamic water	Sluijs *et al.*, 2005
Goniodomids	Warm, lagoonal, water column stratification, high primary productivity	Sluijs *et al.*, 2005; Frieling and Sluijs, 2018
Hystrichosphaeridium	Mid-shelf, cooler temperatures	Frieling and Sluijs, 2018
Impagidinium	Oceanic, offshore, oligotrophic	Sluijs *et al.*, 2005
Membranophoridium perforatum	Mid-shelf	Sluijs *et al.*, 2005
Nematosphaeropsis	Outer neritic	Prebble *et al.*, 2013
Operculodinium	Outer neritic to mid-shelf	Sluijs *et al.*, 2005; Prebble *et al.*, 2013
Palaeocystodinium	Unknown	-
Phthanoperidinium	Fresh-water input	Brinkhuis *et al.*, 2006
Protoperidinium	High nutrients, prey species, high temperature?	Frieling and Sluijs, 2018
Senegalinium	High primary productivity, fresh-water input, cool temperatures	Frieling and Sluijs, 2018
Spiniferites	Cosmopolitan, outer neritic-open marine	Sluijs *et al.*, 2005; Frieling and Sluijs, 2018
Thalassiphora pelagica	Water column stratification	Pross and Schmiedl, 2002
Vozzhennikovia	Cold water	Warnaar *et al.*, 2009
Wetzeliellioids	Warm, normal marine, low terrestrial input	Sluijs *et al.*, 2005; Frieling and Sluijs, 2018

observations regarding the outcrops at nearby Isla Riesco, where Selandian sediments of the Chorrillo Chico Formation directly and sharply overlie the Maastrichtian Rocallosa Formation (see section 4.2). Also, in the Calafate Formation, southern Patagonia Argentina, the K/Pg boundary is eroded and the uppermost part of the section was assigned to the latest Maastrichtian (Marenssi *et al*., 2004). In the upper part of the Río Pérez section, the presence of *Eisenackia reticulata*, FO of *Glaphyrocysta delicata*, *Tanyosphaeridium* spp. and *Thalassiphora delicata* suggests that the sampled section extends up to the Thanetian-Selandian boundary, or just into the

Thanetian, although the Thanetian marker species *Apectodinium homomorphum* was not recorded (Fig. 2).

The assemblages are characterized by two successions from *Senegalinium* spp. via *Spinidinium*/ *Vozzhennikovia* to dominance of *Glaphyrocysta* spp., after which *Senegalinium* spp. remains dominant towards the top of the sampled section. The uppermost part of the section shows another increase in abundance of *Glaphyrocysta* spp. (Fig. 4).

4.1.2. Fuentes; Fuentes Formation

The two samples contain a modestly diverse dinoflagellate cyst assemblage (Supplement 1).

Many species found in these samples have long stratigraphic ranges in the Cretaceous, therefore stratigraphic calibration of these samples mainly depends on the absence of some species which would make the samples any older or younger than the early Campanian. Of interest, we note the abundant occurrence of *Trithyrodinium vermiculatum*, a species described from the Santonian of southern Australia, but without a constrained stratigraphic range, and *Amphidiadema denticulata*. *Odontochitina costata* and *O. porifera* are also common. The presence of *Nelsoniella aceras* suggest that the top part of the Fuentes section is of early-mid Campanian age, particularly in absence of the typical upper Campanian-Maastrichtian species of *Manumiella* (Bowman *et al.*, 2012).

4.1.3. Wells T-1 and T-22; Leña Dura and Loreto formations

Two out of the nine samples were barren of dinoflagellate cysts but did contain a diverse terrestrial palynomorph assemblage. The barren samples come from above the Leña Dura/Loreto boundary, and below the thick coal horizon. The samples from the Leña Dura Formation contain diverse and well-preserved dinoflagellate cysts. Species of stratigraphic importance include *Enneadocysta dictyostila*, *E. brevistila*, *E. multicornuta*, *Eocladopyxis peniculata*, *Octodinium askiniae*, and *Turbiosphaera filosa* (Fig. 5). This assemblage corresponds to the SPDZ11/SPDZ12 and the upper part of the zone RTF2 (González Estebenet *et al.*, 2016), which an age ~40±2 Ma. The single sample from the Loreto Formation from T-1 that yielded dinoflagellate cysts, lacks *Enneadocysta multicornuta*, *E. brevistila* and *Turbiosphaera filosa*, but contains *Stoveracysta ornata*, which tentatively suggests a younger age (36.7-32.1 Ma; Houben *et al.*, 2019). U-Pb Zircon ages from a sandstone sample from the base of the Loreto Formation from Well T-22 shows a highly unimodal signature with ~80% of the 93 analyzed grains falling in the ~36 to ~40 Ma age range (Fig. 5). Samples yield a TuffZirc ^{206}Pb/^{238}U age of 38.1±0.5 Ma (n=73, 2σ). Minor subordinate Cretaceous peaks (81-121 Ma) are present. The age for the T-22 zircons is therefore broadly consistent with the dinoflagellate cyst ages. Dinoflagellate cyst assemblages are dominated by *Enneadocysta* spp. and the *Spinidinium/Vozzhennikovia* group, representing dominantly endemic taxa characteristic of mid-shelf conditions (Fig. 5).

4.2. Isla Riesco región

4.2.1. North-coastal outcrops Isla Riesco; Rocallosa, Chorillo Chico, Agua Fresca, Tres Brazos formations

The dinoflagellate cyst assemblages from this region confirm the tentatively suggested ages for the respective formations. From our samples, termed CAPO, from the Rocallosa Formation, we could not retrieve any dinoflagellate cysts. This testifies to the oxidative nature of the sedimentary regime, which might still have been marine in nature. The sediments from the directly overlying Chorrillo Chico Formation (CC) contain diverse marine dinoflagellate cyst assemblages including *Leptodinium pustulatum*, *Apectodinium homomorphum* and *Eisenackia reticulata* (Supplement 1), which indicate a mid-Selandian age (Table 3; Fig. 2). The two samples from the Agua Fresca Formation that we analyzed also yield a diverse dinoflagellate cyst assemblage with abundant (>50%) *Apectodinium homomorphum*, a questionable specimen of *Muratodinium fimbriatum* and *Hystrichokolpoma rigaudiae*, tentatively placing these samples close to the Paleocene-Eocene boundary; although carbon isotope stratigraphy on a high-resolution sample set would be required to confirm the presence of the Paleocene-Eocene Thermal Maximum (Sluijs and Brinkhuis, 2009). The samples from Tres Brazos Formation are dominated by terrestrial organic matter and palynomorphs, the dinoflagellate cyst species present include *Cleistosphaeridium polypetellum*, which assigns the age of these samples to dinoflagellate cyst zone SPDZ3-5, mid-Ypresian (54-51.7 Ma; Bijl *et al.*, 2013b).

4.2.2. Well SELK-65; Leña Dura Formation

All samples contain abundant, diverse and well-preserved dinoflagellate cysts. Species of stratigraphic importance include *Cleistosphaeridium diversispinosum*, *Dapsilidinium pastielsii*, *Enneadocysta brevistila*, *E. pectiniformis*, *Eocladopyxis peniculata*, *Hystrichosphaeridium tubiferum*, *Impagidinium victorianum*, *Octodinium askiniae* and *Vozzhennikovia roehliae* (Fig. 6). This assemblage, plus the absence of *Membranophoridium perforatum*, *Turbiosphaera filosa* and *Homotryblium tasmaniense* allows us to assign this section to the upper SPDZ12-lower SPDZ13 of Bartonian age (Fig. 6). It also correlates to the upper part of zone RTF2, which according to Guerstein *et al.* (2014)

includes the Middle Eocene Climatic Optimum, a global warming phase of about 500,000 years dated at ~40 Ma (Bohaty and Zachos, 2003; Bohaty *et al*., 2009; Cramwinckel *et al*., 2018). Unfortunately, typical marker species for the MECO, such as *Dracodinium rhomboideum* and *Lophocysta* spp., found elsewhere in association with the MECO, including the Southern Ocean (Bijl *et al*., 2013b), could not be positively identified. Assemblages are dominated by *Enneadocysta* spp., with a good representation of *Thalassiphora pelagica* at the bottom and the middle part of the section (Fig. 6), and the total assemblage suggests a relatively deep, mid-shelf depositional setting for the region.

4.2.3. Río Los Palos; Loreto Formation

The samples from this outcrop generally contain diverse, well-preserved and occasionally superabundant dinoflagellate cysts. Two samples (at 115 and 129 m stratigraphic height) did not contain any dinoflagellate cysts and imply terrestrial depositional environments. The dinoflagellate cyst taxa include *Brigantedinium simplex* (FO halfway the section), *Cleistosphaeridium diversispinosum* (LO halfway the section), *Octodinium askiniae* (LO towards the top of the section), and *Turbiosphaera sagena* (FO halfway the section; Fig. 7). The presence of *Brigantedinium simplex* and *Turbiosphaera sagena* corresponds to the SPDZ15 dinoflagellate cyst zone (Houben *et al*., 2019), which is dated 35.7 Ma. This is in agreement with isotopic ages from zircon grains from the upper part of the Loreto Formation cropping out in the Brunswick Peninsula indicates an age of 36.48±0.47 Ma (Otero *et al*., 2012). Abundant *Spinidinium macmurdoense*, *Vozzhennikovia apertura* and *Turbiosphaera sagena* (Fig. 7) are consistent with a shelf depositional setting.

4.3. Brunswick Peninsula region

4.3.1. Well RGP-03; Tres Brazos Formation

Abundance of dinoflagellate cysts varies in the 29 samples we examined, but all contain dinoflagellate cysts. Ubiquitous also are terrestrial palynomorphs. Dinoflagellate cyst assemblages are diverse, well-preserved and contain many stratigraphically significant species: *Apectodinium homomorphum*, *Batiacasphaera cassiculus*, *Cleistosphaeridium diversispinosum*, *C. polypetellum*, *Manumiella*

rotunda, *Membranophoridium perforatum*, *Octodinium askiniae* and *Selenopemphix nephroides* (Fig. 8; Table 3). The coeval occurrence of these species indicates dinoflagellate cyst zone SPDZ6/SPDZ7 (late Ypresian; ~51.5-49.0 Ma), also supported by the absence of *Palaeocystodinium golzowense,* of which the LO defines the base of SPDZ6, and the FO's of *Turbiosphaera filosa* and *Enneadocysta dictyostila* higher up in the sequence. This implies that *Manumiella rotunda*, the only taxon that suggests an older age, is either reworked from older strata or has a longer stratigraphic range here than in the Pacific Ocean. Unfortunately, *Danea crassimurata*, the FO of which defines the SPDZ6/7 zone boundary, was not recognized at this site. The assemblages are dominated by *Senegalinium* spp., *Vozzhennikovia*/*Spinidinium* spp., and *Deflandrea antarctica* (Fig. 8). One of the authors (GRG) recorded very similar assemblages in equivalent sediments of Patagonian Argentina, from outcrops of the lower member of the Río Turbio Formation in Estancia Cancha Carrera (Fig. 1).

4.3.2. Pecket Mine; Loreto Formation

While all eight analyzed samples contain abundant terrestrial palynomorphs, only 3 yield dinoflagellate cysts, of which one contained too few for assemblage analyses. This suggests that the succession reflects very near-shore to terrestrial depositional environment. The two productive samples for dinoflagellate cysts contain a diverse assemblage with *Brigantedinium simplex*, *Enneadocysta dictyostila*, *Glaphyrocysta semitecta*, *Hystrichokolpoma rigaudiae*, *Lejeunecysta* spp., *Operculodinium* spp., *Selenopemphix* brinkhuisii, abundant *Spinidinium macmurdoense*, and *Turbiosphaera sagena* (Fig. 9). *T. sagena* is a distinct morphotype of a *T. filose-T. sagena* continuum, termed the *T. filosa* complex. In the Río Turbio area, the FO of *T. sagena* coincides with the FCO of the *T. filosa* complex (Guerstein, personal observation, 2020). The abundance of *T. sagena* may make this section slightly younger than that of Río Los Palos at Isla Riesco, where *T. sagena* only sporadically occurs. This assemblage correlates to the lowermost part of zone RTF4 considered to range from middle to late Priabonian in age (Fig. 2). Zone RTF4 contains the transition from abundant endemic-Antarctic species to dominant cosmopolitan taxa, with high amounts of protoperidinaceans, *Nematosphaeropsis* spp. This shift in the dinoflagellate

cyst assemblage composition may be linked to the widening of the Drake Passage and the Tasman Gateway (Sluijs *et al*., 2003; Sijp *et al*., 2016) and invigoration of surface currents (Houben *et al*., 2019), leading to redistribution of heat and potentially moisture. The presence of *Selenopemphix brinkhuisii* tentatively places this section into the early Oligocene. However, the FO of this species is close to the base of the section overlying a 14 Myr long hiatus at Integrated Ocean Drilling Program Site U1356 at the Wilkes Land Margin, Antarctica (Bijl *et al.*, 2018), which means that the true FO of *S. brinkhuisii* may be older. We did not record other typical markers for the early Oligocene, such as the regionally calibrated *Malvinia escutiana* (Houben *et al*., 2011). Moreover, from the Pecket Mine tephra sample, which is stratigraphically below the occurrence of *S. brinkhuisii*, U-Pb results for 45 zircon grains from sample Pecket yield a TuffZirc ^{206}Pb/^{238}U age of 36.6±0.7 Ma (Fig. 9).

5. Discussion

5.1. Ages of formations

The combined results of dinoflagellate cyst biostratigraphy and U-Pb radiometric dating has improved the stratigraphic ages of sedimentary formations of the Austral-Magallanes basin (Fig. 10). Using the results from this study, combined with selected previous biostratigraphic results (*e.g*., Malumián *et al*., 2013), it appears that periods of non-deposition or hiatuses occur during the mid-Campanian-Maastrichtian, Danian, mid-Ypresian, Ypresian-Lutetian and Rupelian.

The mid-Campanian-Maastrichtian hiatus is suspected because the top of the Fuentes Formation is early to mid-Campanian and not Maastrichtian as was suggested earlier (Malumián *et al.*, 2013), while the overlying Rocallosa Formation is late Maastrichtian in age (Malumián *et al*., 2013). Thomas (1949)
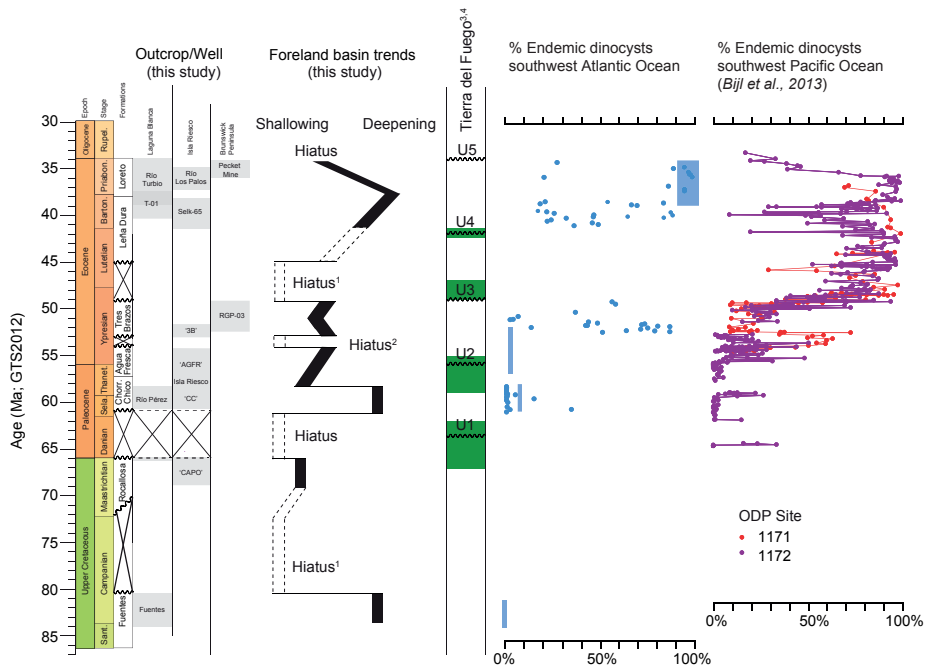

FIG. 10. Stratigraphic interpretation of our study. Epochs, Stages, Formations, and the ages of the studied sections. We deduced a composite record of the relative water depth trends and sedimentary hiatuses, also based on Thomas (1949; hiatus 1) and Malumian *et al.* (2013; hiatus 2), which compare well known intervals of tectonic compression (green shading) and sedimentary hiatuses (wiggly lines) from the Fuegian Andes (Torres Carbonell *et al*., 2013, 2014). Based on these age constraints, we present a composite record of the relative abundance of endemic-Antarctic dinoflagellate cysts in Chilean (this study) and Argentinian (Guerstein *et al*., 2014; González Estebenet *et al*., 2016; blue boxes) southern Patagonia and compare to the southwest Pacific Ocean (Bijl *et al*., 2013b, 2014).

already noted an unconformable superposition of the Rocallosa Formation over Fuentes Formation. The duration of the hiatus is as yet poorly resolved: our study did not successfully date the base of the Rocallosa Formation. Based on the radiometric dates reported in Malumián *et al.* (2013) for the Rocallosa Formation, we deduce an early Maastrichtian age for the base of that formation.

The boundary between Rocallosa and Chorillo Chico formations. represents a hiatus, which, at our studied sections, straddles the Danian and into the early Selandian (~66-61 Ma). The boundary to the overlying Agua Fresca Formation was not recovered, but the samples from Agua Fresca at Isla Riesco revealed an age close to the Paleocene/Eocene boundary. Malumián *et al.* (2013) presented planktonic and foraminifera dating suggesting the Agua Fresca Formation extends well into the Ypresian.

The early Eocene (52-49 Ma) age for the Tres Brazos Formation from the north shore of Isla Riesco is at odds with previous ages for this formation by Malumián *et al.* (2013) (45-42 Ma). Typical dinoflagellate cysts for such a young age (*e.g.*, *Enneadocysta* spp.) are absent in the samples of Tres Brazos Formation we studied (*e.g.*, RGP-3). Although we did not observe the boundary between these units, Malumián *et al.* (2013) described the boundary between Agua Fresca and Tres Brazos formations as unconformable. Based on our older ages for the Tres Brazos Formation, we here infer that the unconformable contact between Agua Fresca and Tres Brazos formations may not represent much more than 1 Myr.

The Ypresian-Lutetian hiatus of around 4 Myr separates the Tres Brazos Formation, with a youngest age of 49 Ma, from the Leña Dura Formation, with an oldest possible age of 45 Ma, based on the common abundance of *Enneadocysta* spp. This interpretation disagrees with the proposed by Malumián *et al.* (2013), who placed these formations conformably. Importantly, however, Thomas (1949) described the boundary between the Tres Brazos and Leña Dura formations as clearly non-conformable, which would support an older age for the Tres Brazos Formation, and a hiatus in between. Based on the continuous common abundance of *Enneadocysta* spp. (Bijl *et al.*, 2013b), the age of the base of the Leña Dura Formation is not older than ~45 Ma, which suggests an Ypresian-Lutetian hiatus of 4 Myr. Collectively, however, the total maximum

age span of the Tres Brazos Formation is uncertain and may vary considerably over the region because of tectonic deformation and hiati (*e.g.*, Thomas, 1949; Malumián *et al.*, 2013; Torres Carbonell *et al.,* 2013).

The zircons and dinoflagellate cysts of the Pecket Mine tephra shows a late Eocene (Priabonian) depositional age for the base of the section, consistent with the proposed age for the Loreto Formation by Otero *et al.* (2012). The zircon sample from well T-22, representing the basal Loreto Formation, has a very strong peak at 38 Ma, which is interpreted as a maximum deposition age. This is also in agreement with the dinoflagellate cyst-based ages and corresponds to the age range for the boundary between Leña Dura and Loreto formations. The subordinate Cretaceous peak (11 grains) (Fig. 5), points to the detrital source of the Loreto Formation sediments. These dates agree with source ages suggested by Fosdick *et al.* (2011), for the Loreto Formation (late Cretaceous, early Cretaceous and late Jurassic), which suggest that by the late Eocene, these Mesozoic rocks were uplifted in the Andean orogeny.

5.2. Depositional setting and subsidence history

Late Cretaceous and Cenozoic subsidence of oceanic plates underneath the South American Plate, and the resulting uplift of the Fuegian Andes provided continuous subsidence of the Andean Foreland Basin, which created deep depocentres (Olivero and Martinioni, 2001; Somoza and Ghidella, 2012). Meanwhile, the South American plate was under a constant compressional regime during the Campanian-Eocene (Maffione *et al.*, 2015), which caused uplift, folding and thrusting of those same sediments (Torres Carbonell *et al.*, 2013, 2014). The interplay between foreland basin subsidence, compression in the overriding plate, and sediment supply thus governed sedimentation history in the foreland basin.

We infer that the hiatuses in the sedimentary succession signify time intervals before which sedimentation rates had exceeded foreland basin deepening. For instance, while the Leña Dura Formation consists of relatively deep-marine sediments, the overlying Loreto Formation seems to grade from marine coastal into a terrestrial (fluvial) depositional regime towards the latest Eocene. Apparently, either subsidence stalled, sediment supply rates increased and/or compression invigorated that caused a decrease in accommodation space in the foreland basin.

In contrast, during the Maastrichtian, Thanetian-Ypresian, and Bartonian-Priabonian, subsidence rates exceeded sedimentation rates and sediment supply. We base this on the gradual fining upwards of Rocallosa Formation, and stratigraphically expanded shallow-marine sediment packages in the Paleocene Chorrillo Chico and Eocene Agua Fresca, Leña Dura and Loreto formations, respectively, with the latter transitions into non-marine deposits (Figs. 9, 10). The deepest marine successions were deposited during the Selandian and Bartonian deposition of the Chorrillo Chico and Leña Dura formations: sediments are consistently marine, mid-shelf, without interruptions of terrestrial sediments. This suggests that subsidence rates reached a maximum during these time intervals. The timing of a deep foreland basin in the Bartonian corresponds with a switch in sediment provenance: detrital input from eroding young Patagonian batholiths was dammed by the uplift of older Darwin Cordillera thrust sheets inboard of these batholiths (Barbeau *et al.*, 2009). Either the switch in detrital source decreased sediment supply, or the increased uplift of the Darwin-Cordillera complex deepened the foreland basin. Although the timing of a deep foreland basing coincides with this provenance shift, no such shift is observed that could explain the deep mid-Paleocene foreland basin. Throughout the Upper Cretaceous to middle Eocene, sand provenance is consistently from the Patagonian-Fuegan magmatic arc (Barbeau *et al.*, 2009).

Interestingly, the timing of the hiatuses we infer throughout the late Cretaceous-early Oligocene correspond to those found independently in the Fuegian Andes foreland (Torres Carbonell *et al.*, 2013, 2014; Fig. 10) for which also detailed reconstructions of the compressional phases were made. The large-scale spatial consistency between our three study areas and the Fuegian foreland suggests that these hiatuses were forced by tectonics and basin fill dynamics rather than local disturbances at our individual study sections.

In turn, our reconstructed foreland basin depth history is the product of the uplift Andean orogeny, which in turn is governed by subduction rates of the oceanic plates. Tectonic reconstructions reveal fast subduction of the Phoenix plate from 47 Ma onwards (Somoza and Ghidella, 2012), which increased Andean uplift rates in the region and in that process increased subsidence rates in the foreland basin, creating more marine depositional settings at that time. Indeed, our foreland basin depth reconstruction shows a noticeable deepening between the early Eocene Tres Brazos Formation and the mid-middle Eocene Leña Dura Formation (Fig. 10), in line with signs of increased subsidence and thereby, more uplift. Whether the relatively deep marine facies in the mid-Paleocene Andean Foreland basin is also associated with increased subduction rates is still elusive, but our results certainly suggest this.

5.3. Antarctic-endemic dinoflagellate cyst community

The results from Chilean Patagonia presented here show a remarkably similar abundance and evolution of endemic dinoflagellate cysts to that in the southwest Pacific Ocean (Figs. 10, 11): sporadic occurrences of elements of the endemic community during the Paleocene (*Spinidinium* and *Vozzhennikovia*), a brief interval of higher abundances of endemic dinoflagellate cysts during the mid-early Eocene, and then a pronounced proliferation of endemic dinoflagellate cysts from around 52 Ma onwards (although the latter is poorly constrained due to incomplete stratigraphic coverage of the late Ypresian). Previous palynological studies of middle to upper Eocene units from the Austral Basin in Argentina (Fig. 11; Guerstein *et al.*, 2014; González Estebenet *et al.*, 2016) showed a good analogy of the evolution of the Antarctic-endemic assemblage in the southwest Atlantic Ocean with that proposed for the southwest Pacific Ocean by Bijl *et al.* (2013a). Also, the interruption of dominance of endemic dinoflagellate cysts in the middle Eocene as was seen in the southwest Pacific Ocean (Bijl *et al.*, 2011, 2013a), seems to be replicated in the southwest Atlantic (Fig. 10).

Even on a species level, there is no noticeable distinction between dinoflagellate cyst assemblages from the southwest Pacific and the southwest Atlantic. In fact, dinoflagellate cyst assemblages from our study are much more similar to those from the southwest Pacific than to those from the southeast Indian Ocean (Bijl *et al.*, 2011; Houben *et al.*, 2019), despite the suggested oceanographic connection of the southwest Atlantic and southeast Indian Ocean by the large proto-weddell Gyre (Huber *et al.*, 2004; Sijp *et al.*, 2016).

The circum-Antarctic similarity of assemblage character and species composition has several
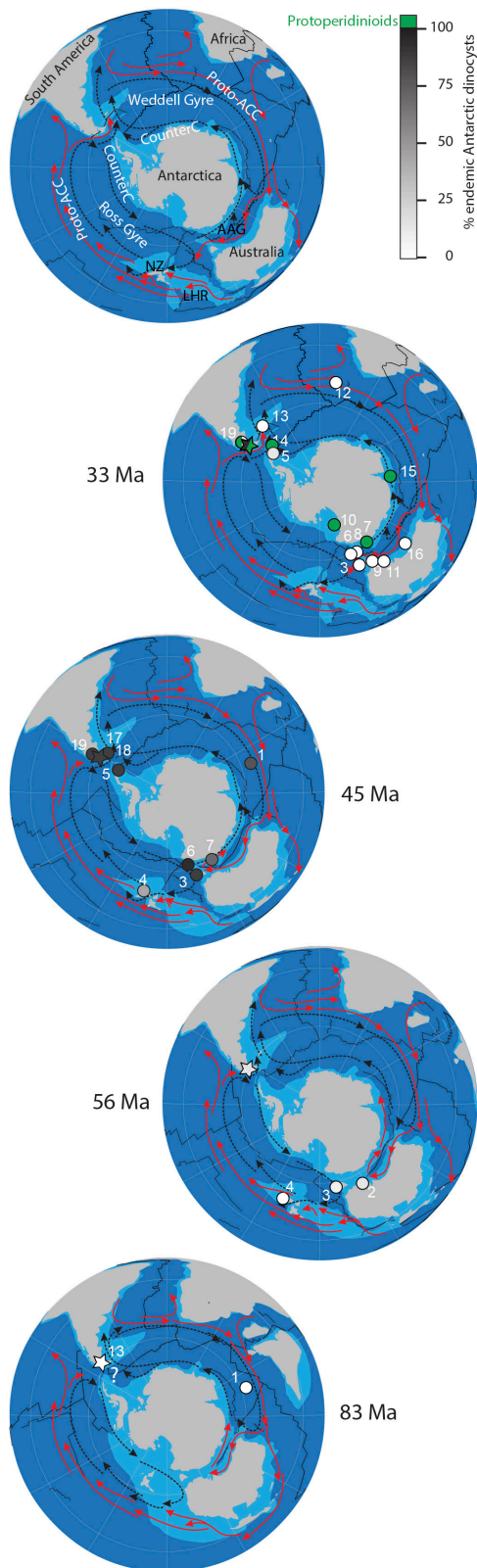
FIG. 11. Paleogeography of the Southern Hemisphere, for 83 Ma, 56 Ma, 45 Ma, and 33 Ma. The plate circuit used is according to Seton *et al.* (2012) on a paleomagnetic reference frame (mid-ocean ridges are indicated in solid black lines). Study area indicated with a star. Arrows indicate low-latitude-derived, subtropical surface currents (red) and Antarctic-derived, polar currents (dashed black). Dots represent locations of dinoflagellate cyst assemblage data from ~5 Myr bins surrounding the time of the respective paleogeographic reconstruction: 85-80 Ma, 58-53 Ma, 47-42 Ma, 34-30 Ma. **NZ:** New Zealand, **LHR:** Lord Howe Rise, **CounterC:** countercurrent, **AAG:** Australo-Antarctic Gulf, **protoACC:** proto-Antarctic Circumpolar Current. Fill gray-scale indicates relative abundance of endemic dinoflagellate cysts, green fill indicates dominance of protoperidinioid dinoflagellate cysts, based on the original papers or reassessed as in Bijl *et al.* (2011): **1.** Site 748 (Mao and Mohr, 1992; P.K. Bijl, personal observation, 2020); **2.** Otway Basin, Australia (Frieling *et al.*, 2018); **3.** ODP Site 1172 (Brinkhuis *et al.*, 2003b; Bijl *et al.,* 2013b; Houben *et al.*, 2019); **4.** Waipara, Tawanui, Ashley Mudstone and Hampden Beach (Crouch and Brinkhuis, 2005; Hollis *et al.,* 2014; Crouch *et al.,* 2014; Dallanave *et al.*, 2016; Cramwinckel *et al.*, 2019); **5.** Seymour Island (Wrenn and Hart, 1988; Douglas *et al.*, 2014; Aménabar *et al.*, 2019); **6.** ODP Site 1171 (Bijl *et al.*, 2013b); **7.** IODP Site U1356 (Bijl *et al.*, 2013b); **8.** ODP Site 1170 (Cramwinckel *et al.,* 2019); **9.** ODP Site 1168 (Brinkhuis *et al.*, 2003a; Sluijs *et al.*, 2003); **10.** CRP-3 (Houben *et al.*, 2013); **11.** Browns Creek (Houben *et al.*, 2019); **12.** ODP Site 1090 (Warnaar, 2006); **13.** ODP Site 511 (Houben *et al.*, 2011, 2019); **14.** ODP Site 696 (Houben *et al.*, 2013, 2019); **15.** ODP Site 739 (Houben *et al.*, 2013); **16.** ODP Site 1128 (Houben *et al.*, 2019); **17.** Leticia Formation, Tierra del Fuego (Guerstein *et al.*, 2008); **18.** Man Aike Formation (Guerstein *et al.*, 2014); **19.** Río Turbio Formation (González Estebenet *et al.*, 2016).

implications. First of all, it precludes geographical isolation of the southwest Pacific Ocean-notably through closure by the poorly constrained bathymetric heights of Zealandia/Lord Howe Rise-as cause for the proliferation of endemism in the Southern Ocean (Bijl *et al.*, 2011; Cramwinckel *et al.*, 2019; Fig. 11). This makes explaining why endemism in the Southern Ocean occurs more difficult. Secondly, it suggests that both southwest Atlantic and southwest Pacific regions were in oceanographic communication with each other. For the middle and late Eocene, this connection is most likely through the counterclockwise flowing Counter Current along coastal Antarctica and connects the proto-Ross Gyre with the proto-Weddell Gyre (Fig. 11; Guerstein *et al.*, 2010; Bijl *et al.*, 2013a; Houben *et al.*, 2019). Ocean model simulations have suggested that the counter-current was most effectively transporting surface waters from the southwest Pacific Ocean westward when Drake Passage was closed (Sijp *et al.*, 2016), which

indeed seems to have been the case at least until 41 Ma (Scher and Martin, 2006). However, during the Paleocene and early Eocene, the counter current was not yet established as the Tasmanian Gateway was seemingly still closed (Exon *et al*., 2004; Bijl *et al*., 2013a), yet endemic species were present in both the southwest Pacific (Bijl *et al*., 2011, 2013a, b) and southwest Atlantic oceans (this study). While Wrenn and Beckmann (1982) interpreted these patterns as evidence for a transantarctic seaway between East and West Antarctica, the latest paleotopographic reconstructions of Antarctica (*e.g*., Wilson *et al*., 2012; Paxman *et al*., 2019) leave little room for a marine transantarctic connection. The easiest way the synchronous proliferation of dinoflagellate cyst endemism in both South Atlantic and Pacific basins is that Drake Passage must have been shallowly open throughout at least the Paleocene and Eocene. This would make the eastward throughflow through Drake Passage as reconstructed by Scher and Martin (2006) reflective of a widening/deepening of Drake Passage, allowing also deep waters of both basins to be connected. This interpretation corroborates with the distinctly different sediment provenance signatures in the Antarctic Larsen basin and the then adjacent Austral basin in Patagonia, which also tentatively suggested early tectonic separation (Barbeau, 2013).

6. Conclusions

Our study places key sedimentary formations in the South Patagonian foreland basin into an absolute time frame, identifies and dates phases of accelerated subsidence of these basins, and reconstructs the paleoceanographic consequences of Campanian-Eocene tectonic events. We recognize regional sedimentary hiatuses spanning the late Campanian, early-to mid-Paleocene, mid-Eocene and latest Eocene-early Oligocene, indicating phases of increased sedimentation in and/or ceased subsidence/ increased compression of the foreland basin. The time intervals in between these compressional phases are characterized by thick successions of mid-to inner shelf marine and terrestrial sedimentary regimes, notably the early Campanian, mid-Paleocene, Paleocene-Eocene boundary and middle Eocene, which represent phases of increased subsidence. The dinoflagellate cyst assemblages suggest the region was under the influence of the Antarctic-derived suface waters driven by the western boundary

currents of the proto-Weddell gyre throughout. Furthermore, the consistent evolution of endemic-Antarctic dinoflagellate cysts in both the southwest Pacific and the southwest Atlantic suggests continued oceanic connectivity since the Paleocene, perhaps through a continuous shallow southern opening in an incipiente Drake Passage.

Acknowledgements

References

Amenábar C.R.; Montes, M.; Nozal, F.; Santillana, S. 2019. Dinoflagellate cysts of the La Meseta Formation (middle to late Eocene), Antarctic Peninsula: Implications for biostratigraphy, paleoceanography and palaeoenvironment. Geological Magazine 157 (3): 351-366. doi: 10.1017/S0016756819000591.

Askin, R.A. 1988. Campanian to Paleocene palynological succession of Seymour and adjacent islands, northeastern Antarctic Peninsula. Geological Society of America, Memoir 169: 131-153.

Awad, W.K.; Oboh-Ikuenobe, F.E. 2016. Early Paleogene dinoflagellate cysts from ODP Hole 959D, Côte d'Ivoire-Ghana Transform Margin, West Africa: New species, biostratigraphy and paleoenvironmental implications. Journal of African Earth Sciences 123: 123-144.

Barbeau, D.L.; Olivero, E.B.; Swanson-Hysell, N.L.; Zahid, K.M.; Murray, K.E.; Gehrels, G.E. 2009. Detrital-zircon geochronology of the eastern Magallanes foreland basin: Implications for Eocene kinematics of the northern Scotia Arc and Drake Passage. Earth and Planetary Science Letters 284 (3-4): 489-503. doi: 10.1016/j.epsl.2009.05.014.

Barker, P.F.; Thomas, E. 2004. Origin, signature and paleoclimatic influence of the Antarctic Circumpolar Current. Earth Science Reviews 66: 143-162.

Barker, P.F.; Dieckmann, B.; Escutia, C. 2007. Onset of Cenozoic Antarctic glaciation.Deep Sea Research, Part II: Topical Studies in Oceanography 54 (21-22): 2293-2307. doi: 10.1016/j.dsr2.2007.07.027.

Bijl, P.K.; Pross, J.; Warnaar, J.; Stickley, C.E.; Huber, M.; Guerstein, R.; Houben, A.J.P.; Sluijs, A.; Visscher, H.; Brinkhuis, H. 2011. Environmental forcings of Paleogene Southern Ocean dinoflagellate biogeography. Paleoceanography 26: PA1202.

Bijl, P.K.; Bendle, A.P.J.; Bohaty, S.M.; Pross, J.; Schouten, S.; Tauxe, L.; Stickley, C.E.; McKay, R.M.; Röhl, U.; Olney, M.; Sluijs, A.; Escutia, C.; Brinkhuis, H.; Expedition 318 scientists. 2013a. Eocene cooling linked to early flow across the Tasmanian Gateway. Proceedings of the National Academy of Sciences of the United States of America 110: 9645-9650.

Bijl, P.K.; Sluijs, A.; Brinkhuis, H. 2013b. A magneto-chemo-stratigraphically calibrated dinoflagellate cyst zonation of the early Paleogene South Pacific Ocean. Earth-Science Reviews 124: 1-31.

Bijl, P.K.; Brinkhuis, H.; Egger, L.M.; Eldrett, J.S.; Frieling, J.; Grothe, A.; Houben, A.J.P.; Pross, J.; Sliwinska, K.K.; Sluijs, A. 2016. Comment on "Wetzeliella and its allies-the "hole" story: a taxonomic revision of the Paleogene dinoflagellate subfamily Wetzelielloideae" by Williams *et al*. (2015). Palynology 41 (3): 423-429. doi: 10.1080/01916122.2016.1235056.

Bijl, P.K.; Houben, A.J.P.; Bruls, A.; Pross, J.; Sangiorgi, F. 2018. Stratigraphic calibration of Oligocene-Miocene organic-walled dinoflagellate cysts from offshore Wilkes Land, East Antarctica, and a zonation proposal. Journal of Micropalaeontology 37: 105-138.

Bohaty, S.M.; Zachos, J.C. 2003. Significant Southern Ocean warming event in the late middle Eocene. Geology 31: 1017-1020.

Bohaty, S.M.; Zachos, J.C.; Florindo, F.; Delaney, M.L. 2009. Coupled greenhouse warming and deep-sea acidification in the Middle Eocene. Paleoceanography and Paleoclimatology 24 (2): PA2207. doi:10.1029/2008PA001676.

Bowman, V.C.; Francis, J.E.; Riding, J.B.; Hunter, S.J.; Haywood, A.M. 2012. A latest Cretaceous to earliest Paleogene dinoflagellate cyst zonation from Antarctica, and implications for phytoprovincialism in the high southern latitudes. Review of Palaeobotany and Palynology 171: 40-56.

Brinkhuis, H.; Biffi, U. 1993. Dinoflagellate cyst stratigraphy of the Eocene/Oligocene transition in Central Italy. Marine Micropaleontology 22: 131-183.

Brinkhuis, H.; Bujak, J.P.; Smit, J.; Versteegh, G.J.M.; Visscher, H. 1998. Dinoflagellate-based sea surface temperature reconstructions across the Cretaceous-Tertiary boundary. Palaeogeography, Palaeoclimatology, Palaeoecology 141: 67-83.

Brinkhuis, H.; Munsterman, D.M.; Sengers, S.; Sluijs, A.; Warnaar, J.; Williams, G.L. 2003a. Late Eocene to Quaternary dinoflagellate cysts from ODP Site 1168, off western Tasmania. *In* Proceedings of the Ocean Drilling Program, Scientific Results 189: 1-48 (Online). United States Government Printing Office, College Station, TX (Ocean Drilling Program): 1-36. doi:10.2973/odp.proc.sr.189.105.2003.

Brinkhuis, H.; Sengers, S.; Sluijs, A.; Warnaar, J.; Williams, G.L. 2003b. Latest Cretaceous to earliest Oligocene, and Quaternary dinoflagellates from ODP Site 1172, East Tasman *Plateau*. *In* Proceedings of the Ocean Drilling Program, Scientific Results (Exon, N.; Kennett, J.P.; editors). United States Government Printing Office, College Station 189: 1-48 (Online). Texas.

Brinkhuis, H.; Schouten, S.; Collinson, M.E.; Sluijs, A.; Sinninghe Damsté, J.S.; Dickens, G.R.; Huber, M.; Cronin, T.M.; Onodera, J.; Takahashi, K.; Bujak, J.P.; Stein, R.; Burg, J.V.D.; Eldrett, J.S.; Harding, I.C.; Lotter, A.F.; Sangiorgi, F.; Konijnenburg-Cittert, H.V.; Leeuw, J.W.D.; Matthiessen, J.; Backman, J.; Moran, K.; Expedition 302 Scientists. 2006. Episodic fresh surface waters in the Eocene Arctic Ocean. Nature 441: 606-609.

Brown, S.; Downie, C. 1984. Dinoflagellate cyst biostratigraphy of late Paleocene and early Eocene sediments from Holes 552, 553A, and 555, Leg 81, Deep Sea Drilling Project (Rockall *Plateau*). Initial Reports DSDP, Leg 81, Southampton to Azores: 565-579. doi: 10.2973/dsdp.proc.81.113.1984.

Bujak, J.P.; Mudge, D.C. 1994. A high-resolution North Sea Eocene dinocyst zonation. Journal of the Geological Society 151 (3): 449-462. London.

Chang, Z.; Vervoort, J.D.; McClelland, W.C.; Knaack, C. 2006. U-Pb dating of zircon by LA-ICP-MS. Geochemistry, Geophysics, Geosystems 7: Q05009.

Charrier, R.; Lahsen, A. 1969. Stratigraphy of Late Cretaceous-Early Eocene of Seno Skyring-Estrecho of Magellan area, Magallanes Province, Chile. American Association of Petroleum Geologists, Bulletin 53 (3): 568-590.

Charrier, R.; Pinto, L.; Rodríguez, M.P. 2007. Tectonostratigraphic evolution of the Andean Orogen in Chile. *In* The Geology of Chile (Moreno, T.; Gibbons, W.; editors). The Geological Society, Special Publication: 21-114. London.

Cookson, I.C.; Cranwell, L.M. 1967. Lower Tertiary microplankton, spores and pollen grains from southernmost Chile. Micropaleontology 13: 204-216.

Costa, L.I.; Davey, R.J. 1992. Dinoflagellate cysts of the Cretaceous system. *In* A stratigraphix index of dinoflagellate cysts (Powell, A.J.; editor). British Micropaleontological Society Publication Series: 99-154.

Cramwinckel, M.J.; Huber, M.; Kocken, I.J.; Agnini, C.; Bijl, P.K.; Bohaty, S.M.; Frieling, J.; Goldner, A.; Hilgen, F.J.; Kip, E.L.; Peterse, F.; Van Der Ploeg, R.; Röhl, U.; Schouten, S.; Sluijs, A. 2018. Synchronous tropical and polar temperature evolution in the Eocene letter. Nature 559: 382-386.

Cramwinckel, M.J.; Woelders, L.; Huurdeman, E.P.; Peterse, F.; Gallagher, S.J.; Pross, J.; Burgess, C.; Reichart, G.J.; Sluijs, A.; Bijl, P.K. 2019. Surface-circulation change in the Southern Ocean across the Middle Eocene Climatic Optimum: inferences from dinoflagellate cysts and biomarker paleothermometry. Climate of the Past Discussions 2019: 1-34.

Crouch, E.M.; Brinkhuis, H. 2005. Environmental change across the Paleocene-Eocene transition from eastern New Zealand: A marine palynological approach. Marine Micropaleontology 56: 138-160.

Crouch, E.M.; Willumsen, P.S.; Kulhanek, D.K.; Gibbs, S. 2014. A revised Paleocene (Teurian) dinoflagellate cyst zonation from eastern New Zealand. Palaeogeography, Palaeoclimatology, Palaeoecology 202: 47-79.

Dallanave, E.; Bachtadse, V.; Crouch, E.M.; Tauxe, L.; Shepherd, C.L.; Morgans, H.E.G.; Hollis, C.J.; Hines, B.R.; Sugisaki, S. 2016. Constraining early to middle Eocene climate evolution of the southwest Pacific and Southern Ocean. Earth and Planetary Science Letters 433: 380-392.

Douglas, P.M.J.; Affek, H.P.; Ivany, L.C.; Houben, A.J.P.; Sijp, W.P.; Sluijs, A.; Schouten, S.; Pagani, M. 2014. Pronounced zonal heterogeneity in Eocene southern high-latitude sea surface temperatures. Proceedings of the National Academy of Sciences of the United States of America 111 (18): 6582-6587.

Eagles, G.; Livermore, R.A. 2002. Opening history of Powell Basin, Antarctic Peninsula. Marine Geology 185: 195-205.

Egger, L.M.; Sliwinska, K.K.; van Peer, T.E.; Liebrand, D.; Lippert, P.C.; Friedrich, O.; Wilson, P.A.; Norris, R.D.; Pross, J. 2016. Magnetostratigraphically-calibrated dinoflagellate cyst bioevents for the uppermost Eocene to lowermost Miocene of the western North Atlantic (IODP Expedition 342, Paleogene Newfoundland sediment drifts). Review of Palaeobotany and Palynology 234: 159-185.

Eshet, Y.; Moshkovitz, S.; Habib, D.; Benjamini, C.; Magaritz, M. 1992. Calcareous nannofossil and dinoflagellate stratigraphy across the Cretaceous/Tertiary boundary at Hor Hahar, Israel. Marine Micropaleontology 18: 199-228.

Exon, N.F.; Brinkhuis, H.; Robert, C.M.; Kennett, J.P.; Hill, P.J.; Macphail, M.K. 2004. Tectono-Sedimentary History of Uppermost Cretaceous Through Oligocene Sequences from the Tasmanian Region, A Temperate Antarctic Margin. *In* The Cenozoic Southern Ocean: Tectonics, Sedimentation, and Climate Change between Australia and Antarctica (Exon, N.F.; Kennett, J.P.; Malone, M.J.; editors). Geophysical Monograph Series 151: 319-344.

Firth, J.V. 1996. Upper middle Eocene to Oligocene dinoflagellate biostratigraphy and assemblage variations in hole 913B, Greenland Sea. *In* Proceedings of the Ocean Drilling Program (Thiede, J.; Myrhe, A.M.; Firth, J.V.; Johnson, G.L.; Ruddiman, W.F.; editors). Scientific Results 151: 203-242.

Fosdick, J.C.; Romans, B.W.; Fildani, A.; Bernhardt, A.; Calderón, M.; Graham, S. 2011. Kinematic evolution of the Patagonian retroarc fold-and-thrust belt and Magallanes foreland basin, Chile and Argentina, 51°30′S. Geological Society of America, Bulletin 123 (9-10): 1679-1698.

Frieling, J.; Sluijs, A. 2018. Towards quantitative environmental reconstructions from ancient non-analogue microfossil assemblages: Ecological preferences of Paleocene-Eocene dinoflagellates. Earth-Science Reviews 185: 956-973.

Frieling, J.; Iakovleva, A.I.; Reichart, G.-J.; Aleksandrova, G.N.; Gnibidenko, Z.N.; Schouten, S.; Sluijs, A. 2014. Paleocene-Eocene warming and biotic response in the epicontinental West Siberian Sea. Geology 42 (9): 767-770.

Frieling, J.; Huurdeman, E.P.; Rem, C.C.M.; Donders, T.H.; Pross, J.; Bohaty, S.M.; Holdgate, G.R.; Gallagher, S.J.; McGowran, B.; Bijl, P.K. 2018. Identification of the Paleocene-Eocene boundary in coastal strata

in the Otway Basin, Victoria, Australia. Journal of Micropalaeontology 37: 317-339.

García, F. 1952. Geología de superficie de la parte noroeste de la Isla Riesco. Informe Inédito, Empresa Nacional de Petróleo (ENAP). Santiago.

González Estebenet, M.S.; Guerstein, G.R.; Rodríguez Raising, M.E.; Ponce, J.J.; Alperín, M.I. 2016. Dinoflagellate cyst zonation for the middle to upper Eocene in the Austral Basin, southwestern Atlantic Ocean: Implications for regional and global correlation. Geological Magazine 154: 1022-1036.

Gradstein, F.M.; Kristiansen, I.L.; Loemo, L.; Kaminski, M.A. 1992. Cenozoic foraminiferal and dinoflagellate cyst biostrtigraphy of the central North Sea. Micropaleontology 38-2: 101-137.

Gradstein, F.M.; Ogg, J.G.; Schmitz, M.D.; Ogg, G.M. 2012. The Geologic Time Scale 2012. Elsevier Publishing Company, 2 Volume (Set 1-2): 1-1144.

Guerstein, G.R.; Guler, M.V.; Williams, G.L.; Fensome, R.A.; Chiesa, J.O. 2008. Middle Palaeogene dino-flagellate cysts from Tierra del Fuego, Argentina: Biostratigraphy and palaeoenvironments. Journal of Micropalaeontology 27 (1): 75-94.

Guerstein, G.R.; Guler, M.V.; Brinkhuis, H.; Warnaar, J. 2010. Mid-Cenozoic paleoclimatic and pale-oceanographic trends in the southwestern Atlantic Basins: a dinoflagellate view. *In* The Paleontology of Gran Barranca: Evolution and Environmental Change through the Middle Cenozoic of Patagonia (Madden, R.H.; Carlini, A.A.; Vucetich, M.G.; Kay, R.F.; editors). Cambridge University Press: 1022-1036. London.

Guerstein, G.R.; González Estebenet, M.S.; Alperín, M.I.; Casadio, S.A.; Archangelsky, S. 2014. Correlation and paleoenvironments of middle Paleogene marine beds based on dinoflagellate cysts in southwestern Patagonia, Argentina. Journal of South American Earth Sciences 52: 166-178.

Head, M.J.; Norris, G. 1989. Palynology and dinoflagellate cyst stratigraphy of the Eocene and Oligocene in ODP Leg 105, Hole 647A, Labrador Sea. Proceedings Ocean Drilling Program, Scientific Results, ODP, Leg 105, Baffin Bay and Labrador Sea: 515-550.

Helby, R.; Morgan, R.; Partridge, A.D. 1987. A palyno-logical zonation of the Australian Mesozoic. *In* Studies in Australian Mesozoic Palynology (Jell, P.A.; editor).Association of Australasian Palaeontologists Memoir 4: 1-94.

Hill, P.J.; Exon, N.F. 2004. Tectonics and Basin Development of the Offshore Tasmanian Area; Incorporating Results

from Deep Ocean Drilling. *In* The Cenozoic Southern Ocean; Tectonics, Sedimentation and Climate Change Between Australia and Antarctica (Exon, N.F.; Kennett, J.P.; Malone, M.; editors). American Geophysical Union, Geophysical Monograph Series 151: 19-42. Washington.

Hoffstetter, R.; Fuenzalida, H.; Cecioni, G. 1957. Chili. *In* Lexique Stratigraphique International. Amérique Latine. Centre National de la Recherche Scientifique 5 (7): 444 p. París.

Hollis, C.J.; Tayler, M.J.S.; Andrew, B.; Taylor, K.W.; Lurcock, P.; Bijl, P.K.; Kulhanek, D.K.; Crouch, E.M.; Nelson, C.S.; Pancost, R.D.; Huber, M.; Wilson, G.S.; Ventura, G.T.; Crampton, J.S.; Schiøler, P.; Phillips, A. 2014. Organic-rich sedimentation in the South Pacific Ocean associated with Late Paleocene climatic cooling. Earth-Science Reviews 134: 81-97.

Houben, A.J.P.; Bijl, P.K.; Guerstein, G.R.; Sluijs, A.; Brinkhuis, H. 2011. *Malvinia escutiana*, a new biostratigraphically important Oligocene dinoflagellate cyst from the Southern Ocean. Review of Palaeobotany and Palynology 165: 175-182.

Houben, A.J.P.; Bijl, P.K.; Pross, J.; Bohaty, S.M.; Passchier, S.; Stickley, C.E.; Röhl, U.; Sugisaki, S.; Tauxe, L.; Van De Flierdt, T.; Olney, M.; Sangiorgi, F.; Sluijs, A.; Escutia, C.; Brinkhuis, H. 2013. Reorganization of Southern Ocean plankton ecosystem at the onset of Antarctic glaciation. Science 340: 341-344.

Houben, A.J.P.; Bijl, P.K.; Sluijs, A.; Schouten, S.; Brinkhuis, H. 2019. Late Eocene Southern Ocean cooling and invigoration of circulation preconditioned Antarctica for full-scale glaciation. Geochemistry, Geophysics, Geosystems 20 (5): 2214-2234.

Huber, M.; Brinkhuis, H.; Stickley, C.E.; Döös, K.; Sluijs, A.; Warnaar, J.; Schellenberg, S.A.; Williams, G.L. 2004. Eocene circulation of the Southern Ocean: Was Antarctica kept warm by subtropical waters? Paleoceanography 19: p. PA4026.

Jackson, S.E.; Pearson, N.J.; Griffin, W.L.; Belousova, E.A. 2004. The application of laser ablation-inductively coupled plasma-mass spectrometry to *in situ* U-Pb zircon geochronology. Chemical Geology 211: 47-69.

Lagabrielle, Y.; Goddéris, Y.; Donnadieu, Y.; Malavieille, J.; Suárez, M. 2009. The tectonic history of Drake Passage and its possible impacts on global climate. Earth and Planetary Science Letters 279: 197-211.

Leereveld, H. 1997. Upper Tithonian-Valanginian (Upper Jurassic-Lower Cretaceous) dinoflagellate cyst stratigraphy of the western Mediterranean. Cretaceous Research 18: 385-420.

Livermore, R.; Nankivell, A.; Eagles, G.; Morris, P. 2005. Paleogene opening of Drake Passage. Earth and Planetary Science Letters 236: 459-470.

Ludwig, K.R. 2003. User's manual for Isoplot/Ex version 3.0, a geochronological toolkit for Microsoft Excel. Berkeley Geochronology Center, Special Publication 4: 72 p. California.

Maffione, M.; Hernández-Moreno, C.; Ghiglione, M.C.; Speranza, F.; van Hinsbergen, D.J.J.; Lodolo, E. 2015. Constraints on deformation of the Southern Andes since the Cretaceous from anisotropy of magnetic susceptibility. Tectonophysics 665: 236-250.

Malumián, N.; Hromic T.; Náñez, C. 2013. El Paleógeno de la Cuenca de Magallanes: Biostratigrafía y discontinui-dades. Anales del Instituto de la Patagonia (Chile) 41 (1): 29-52. doi: 10.4067/S0718-686X2013000100003.

Mao, S.; Mohr, B.A.R. 1992. Late Cretaceous dinoflagellate cysts (? Santonian-Maestrichtian) from the Southern Indian Ocean (Hole 748C). *In* Proceedings of the Ocean Drilling Program, Scientific Results (Wise, S.W.; Schlich, R.; editors). Ocean Drilling Program, College Station, TX 120: 307-341. doi: 10.2973/odp.proc. sr.120.190.1992.

Marenssi, S.; Guler, V.; Casadio, S.; Guerstein, R.; Papú, O. 2004. Sedimentology and palynology of the Calafate Formation (Maastrichtian), Austral Basin, Southern Patagonia, Argentina. Cretaceous Research 25: 907-918.

Masure, E.; Rauscher, R.; Dejax, J.; Schuler, M.; Ferre, B. 1998. Cretaceous-Paleocene palynology from the Cote D'ivoire-Ghana Transform Margin, sites 959, 960, 961, and 962. *In* Proceedings of the Ocean Drilling Program (Mascle, J.; Lohmann,G.P.; Moullade, M.; editors). Scientific Results 159: 253-276.

Mohr, B.A.R.; Mao, S. 1997. Maastrichtian dinoflagellate cyst floras from Maud Rise and Georgia Basin (Southern Ocean): Their Stratigraphic and Palaeoenvironmental implications. Palynology 21: 41-65.

Natland, M.L.; González, E.P.; Cañón, A.; Ernst, M. 2014. A System of Stages for correlation of Magallanes Basin Sediments. Geological Society American, Memoir 139: 1-125.

Olivero, E.B.; Martinioni, D.R. 2001. A review of the geology of the Argentinian Fuegian Andes. Journal of South American Earth Sciences 14: 175-188.

Orsi, A.H.; Whitworth III, T.; Nowlin Jr., W.D. 1995. On the meridional extent and fronts of the Antarctic Circumpolar Current. Deep-Sea Research, Part I 42 (5): 641-673.

Otero, R.A.; Torres, T.; Le Roux, J.P.; Hervé, F.; Mark Fanning, C.; Yury-Yáñez, R.E.; Rubilar-Rogers, D. 2012. A Late Eocene age proposal for the Loreto Formation (Brunswick Peninsula, southernmost Chile), based on fossil cartilaginous fishes, paleobotany and radiometric evidence. Andean Geology 39: 180-200. doi: 10.5027/andgeoV39N1-a09.

Paces, J.B.; Miller, J.D. 1993. Precise U-Pb ages of Duluth Complex and related mafic intrusions, northeastern Minnesota: Geochronological insights to physical, petrogenetic, paleomagnetic, and tectonomagmatic processes associated with the 1.1 Ga Midcontinent Rift System. Journal of Geophysical Research, Solid Earth 98: 13997-14013.

Paton, C.; Woodhead, J.D.; Hellstrom, J.C.; Hergt, J.M.; Greig, A.; Maas, R. 2010. Improved laser ablation U-Pb zircon geochronology through robust downhole fractionation correction. Geochemistry, Geophysics, Geosystems 11: Q0AA06. doi: 10.1029/2009GC002618.

Paxman, G.J.G.; Jamieson, S.S.R.; Hochmuth, K.; Gohl, K.; Bentley, M. J.; Leitchenkov, G.; Ferraccioli, F. 2019. Reconstructions of Antarctic topography since the Eocene-Oligocene boundary. Palaeogeography, Palaeoclimatology, Palaeoecology 535: 109346. doi: 10.1016/j.palaeo.2019.109346.

Pérez, L.F.; Hernández-Molina, F. J.; Lodolo, E.; Bohoyo, F.; Galindo-Zaldívar, J.; Maldonado, A. 2019. Oceanographic and climatic consequences of the tectonic evolution of the southern scotia sea basins, Antarctica. Earth-Science Reviews 198: 102922. doi: 10.1016/j.earscirev.2019.102922.

Powell, A.J. 1992. A Stratigraphic Index of Dinofla-gellate Cysts. Chapman and Hall: 290 p. London.

Powell, A.J.; Brinkhuis, H.; Bujak, J.P. 1996. Upper Paleocene-lower Eocene dinoflagellate cyst sequence biostratigraphy of southeast England. *In* Correlation of the Early Paleogene in Northwest Europe (Knox, R.W.O.; Corfield, R.M.; Dunay, R.E.; editors). Geological Societey of Lndon Special Publication 101 (1): 145-183.

Prebble, J.G.; Crouch, E.M.; Carter, L.; Cortese, G.; Bostock, H.; Neil, H. 2013. An expanded modern dinoflagellate cyst dataset for the Southwest Pacific and Southern Hemisphere with environmental associations. Marine Micropaleontology 101: 33-48.

Pross, J.; Schmiedl, G. 2002. Early Oligocene dinoflagellate cysts from the Upper Rhine Graben (SW Germany): paleoenvironmental and paleoclimatic implications. Marine Micropaleontology 45: 1-24.

Pross, J.; Houben, A.J.P.; Simaeys, S.V.; Williams, G.L.; Kotthoff, U.; Coccioni, R.; Wilpshaar, M.; Brinkhuis, H.

2010. Umbria-Marche revisited: A refined magnetostratigraphic calibration of dinoflagellate cyst events for the oligocene of the Western Tethys. Review of Palaeobotany and Palynology 158: 213-235.

Quattrocchio, M.E. 2009. Paleogene dinoflagellate cysts from Punta Prat, southern Chile. Palynology 33: 141-156.

Raine, J.I.; Askin, R.A.; Crouch, E.M.; Hannah, M.J.; Levy, R.H.; Wrenn, J.H. 1997. Palynomorphs. *In* Southern Ocean Late Cretaceous/Early Cenozoic Biostratigraphic Datums (Hannah, M.J.; Raine, J.I.; editors). Institute of Geological and Nuclear Sciences, Scientific Report 97: 25-33.

Sauermilch, I.; Whittaker, J.M.; Bijl, P.K.; Totterdell, J.M.; Jokat, W. 2019. Tectonic, Oceanographic, and Climatic Controls on the Cretaceous-Cenozoic Sedimentary Record of the Australian-Antarctic Basin. Journal of Geophysical Research, Solid Earth 124 (8): 7699-7724.

Scher, H.D.; Martin, E.E. 2006. Timing and Climatic Consequences of the Opening of Drake Passage. Science 312: 428-430.

Sernageomin, 2003. Mapa Geológico de Chile: versión digital. Servicio Nacional de Geología y Minería, Publicación Geológica Digital, No. 4 (Cd-Rom). Santiago.

Seton, M.; Müller, R.D.; Zahirovic, S.; Gaina, C.; Torsvik, T.; Shephard, G.; Talsma, A.; Gurnis, M.; Turner, M.; Maus, S.; Chandler, M. 2012. Global continental and ocean basin reconstructions since 200 Ma. Earth-Science Reviews 113: 212-270.

Sijp, W.P.; von der Heydt, A.S.; Dijkstra, H.A.; Flögel, S.; Douglas, P.M.J.; Bijl, P.K. 2014. The role of ocean gateways on cooling climate on long time scales. Global and Planetary Change 119: 1-22.

Sijp, W.P.; Von Der Heydt, A.S.; Bijl, P.K. 2016. Model simulations of early westward flow across the Tasman Gateway during the early Eocene. Climate of the Past 12: 807-817.

Sláma, J.; Košler, J.; Condon, D.J.; Crowley, J.L.; Gerdes, A.; Hanchar, J.M.; Horstwood, M.S.A.; Morris, G.A.; Nasdala, L.; Norberg, N.; Schaltegger, U.; Schoene, B.; Tubrett, M.N.; Whitehouse, M.J. 2008. Plešovice zircon-A new natural reference material for U-Pb and Hf isotopic microanalysis. Chemical Geology 249: 1-35.

Sliwinska, K.K.; Abrahamsen, N.; Beyer, C.; Brünings-Hansen, T.; Thomsen, E.; Ulleberg, K.; Heilmann-Clausen, C. 2012. Bio-and magnetostratigraphy of Rupelian-mid Chattian deposits from the Danish

land area. Review of Palaeobotany and Palynology 172: 48-69.

Sluijs, A.; Brinkhuis, H. 2009. A dynamic climate and ecosystem state during the Paleocene-Eocene Thermal Maximum: inferences from dinoflagellate cyst assemblages on the New Jersey Shelf. Biogeosciences 6: 1755-1781.

Sluijs, A.; Brinkhuis, H.; Stickley, C.E.; Warnaar, J.; Williams, G.L.; Fuller, M. 2003. Dinoflagellate cysts from the Eocene-Oligocene transition in the Southern Ocean: Results from ODP Leg 189. *In* Proceedings of the Ocean Drilling Program (Exon, N.F.; Kennett, J.P.; Malone, M.J.; editors). Scientific Results 189: 1-42.

Sluijs, A.; Pross, J.; Brinkhuis, H. 2005. From greenhouse to icehouse; organic walled dinoflagellate cysts as paleoenvironmental indicators in the Paleogene. Earth-Science Reviews 68: 281-315.

Somoza, R.; Ghidella, M.E. 2012. Late Cretaceous to recent plate motions in western South America revisited. Earth and Planetary Science Letters 331: 152-163.

Stickley, C.E.; Brinkhuis, H.; Schellenberg, S.A.; Sluijs, A.; Röhl, U.; Fuller, M.; Grauert, M.; Huber, M.; Warnaar, J.; Williams, G.L. 2004. Timing and nature of the deepening of the Tasmanian Gateway. Paleoceanography 19: PA4027. doi: 10.1029/2004PA001022.

Sylvester, P.J.; Ghaderi, M. 1997. Trace element analysis of scheelite by excimer laser ablation-inductively coupled plasma-mass spectrometry (ELA-ICP-MS) using a synthetic silicate glass standard. Chemical Geology 141: 49-65.

Thomas, C. 1949. Geology and petroleum explorations in Magallanes Province, Chile. American Association of Petroleum Geologists, Bulletin 33: 1553-1578.

Tocher, B.A.; Jarvis, I. 1996. Dinoflagellate cyst distri-butions and the Albian-Cenomanian boundary (mid-Cretaceous) at Cordebugle, NW France and Lewes, southern England. Journal of Micropalaeontology 15: 55-67.

Torres Carbonell, P.J.; Dimieri, L.V.; Martinioni, D.R. 2013. Early foreland deformation of the Fuegian Andes (Argentina): Constraints from the strain analysis of Upper Cretaceous-Danian sedimentary rocks. Journal of Structural Geology 48: 14-32.

Torres Carbonell, P.J.; Dimieri, L.V.; Olivero, E.B.; Bohoyo, F.; Galindo-Zaldívar, J. 2014. Structure and tectonic evolution of the Fuegian Andes (southernmost South America) in the framework of the Scotia Arc development. Global and Planetary Change 123: 174-188.

Van Mourik, C.A.; Brinkhuis, H. 2005. The Massignano Eocene-Oligocene golden spike section revisited. Stratigraphy 2: 13-30.

Van Mourik, C.A.; Brinkhuis, H.; Williams, G.L. 2001. Mid-to late Eocene organic-walled dinoflagellate cysts from ODP Leg 171B, offshore Florida. Geological Society of London Special Publication 183: 225-251.

Warnaar, J. 2006. Climatological implications of Australian-Antarctic separation. Ph.D. Thesis (Unpublished). Laboratory of Palaeobotany and Palynology Contributions Series No. 22: 143 p. Utrecht.

Warnaar, J.; Bijl, P.K.; Huber, M.; Sloan, L.C.; Brinkhuis, H.; Röhl, U.; Sriver, R.; Visscher, H. 2009. Orbitally forced climate changes in the Tasman sector during the Middle Eocene. Palaeogeography, Palaeoclimatology, Palaeoecology 280: 361-370.

Williams, G.L.; Stover, L.E.; Kidson, E.J. 1993. Morphology and stratigraphic ranges of selected Mesozoic-Cenozoic dinoflagellate taxa in the Northern Hemisphere. Geolological Survey of Canada 92 (10): 1-137.

Williams, G.L.; Fensome, R.A.; MacRae, R.A. 2017. DINOFLAJ3. American Association of Stratigraphic Palynologists, Data Series 2. http://dinoflaj.smu.ca/dinoflaj3.

Wilson, D.S.; Jamieson, S.S.R.; Barrett, P.J.; Leitchenkov, G.; Gohl, K.; Larter, R.D. 2012. Antarctic topography at the Eocene-Oligocene boundary. Palaeogeography, Palaeoclimatology, Palaeoecology 335-336: 24-34. doi: 10.1016/j.palaeo.2011.05.028.

Wrenn, J.H.; Beckman, S.W. 1982. Maceral, total organic carbon, and palynological analyses of Ross Ice Shelf Project Site J9 cores. Science 216: 187-189.

Wrenn, J.H.; Hart, G.F. 1988. Paleogene dinoflagellate cyst biostratigraphy of Seymour Island, Antarctica. Geological Society of America, Memoires 169: 321-447.

Zegarra, M.; Helenes, J. 2011. Changes in Miocene through Pleistocene dinoflagellates from the Eastern Equatorial Pacific (ODP Site 1039), in relation to primary productivity. Marine Micropaleontology 81: 107-121.
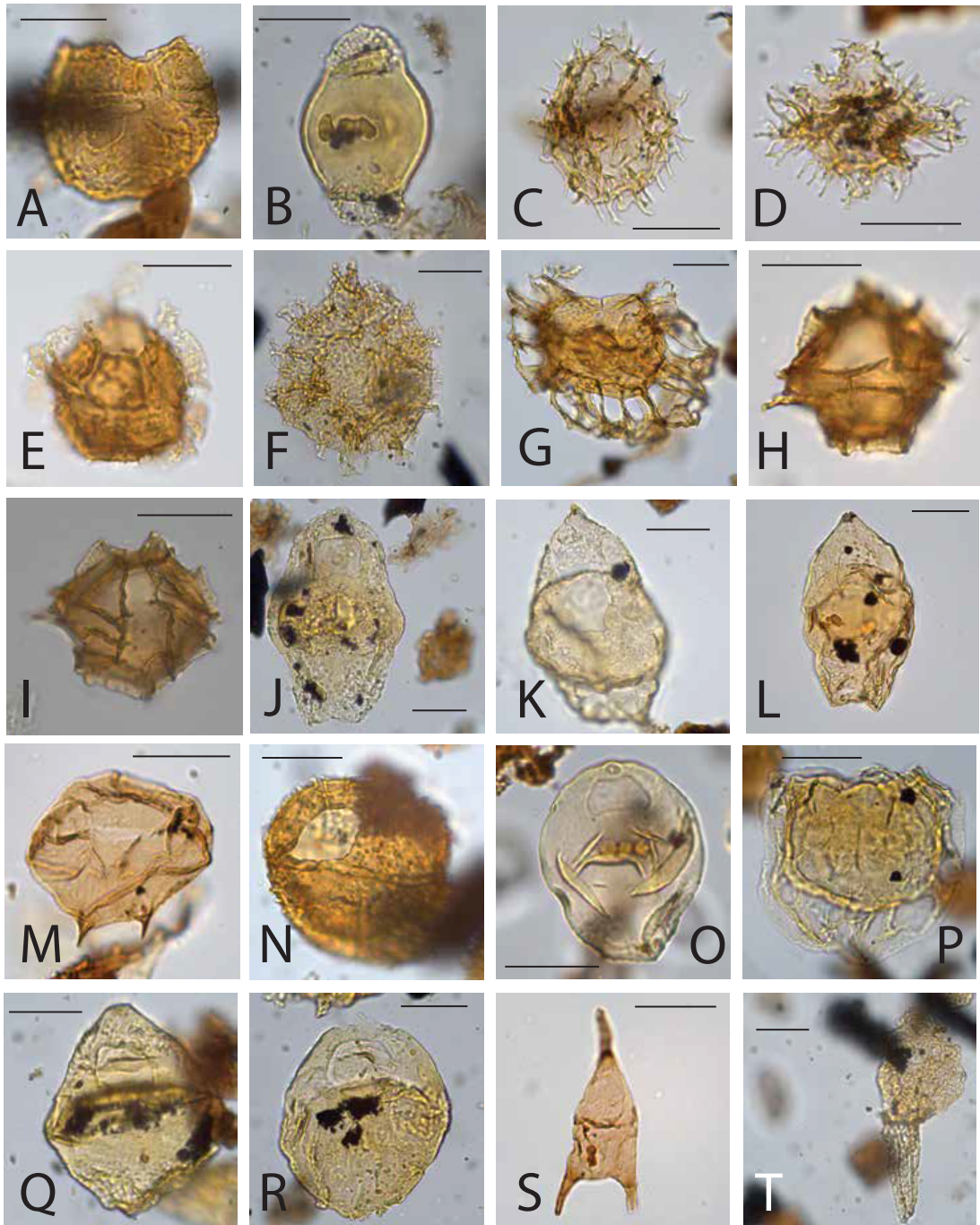
PLATES

PLATE 1. **A.** *Alisocysta margarita* Chorrillo Chico (CC)3; **B.** *Amphidiadema denticulata*, Fuentes (FUEN)1; **C.** *Apectodinium homomorphum*, Agua Fresca (AGFR)3; **D.** *Apectodinium* sp., AGFR1; **E.** *Cassidium filosum*, Río Pérez (RP)13; **F.** *Circulodinium compactum*, FUEN1; **G.** *Glaphyrocysta pastielsii*, RP9; **H-I.** *Impagidinium* sp., RP13; **J.** *Isabelidinium bakeri*, FUEN1; **K.** *Isabelidinium bakeri*, FUEN3; **L.** *Isabelidinium bakeri*, RP6; **M.** *Lejeunecysta fallax*, Pecket Mine (PM)6; **N.** *Leptodinium pustulatum*, CC3; **O.** *Manumiella seymourense*, FUEN3; **P.** *Membranophoridium perforatum*, RGP3-21-1-79; **Q.** *Nelsoniella aceras*, FUEN1; **R.** Nelsoniella aceras, FUEN1; **S.** *Octodinium askiniae*, RGP3-24-1-1; **T.** *Odontochitina cribropoda*, FUEN1; Scale bar=25 μm.
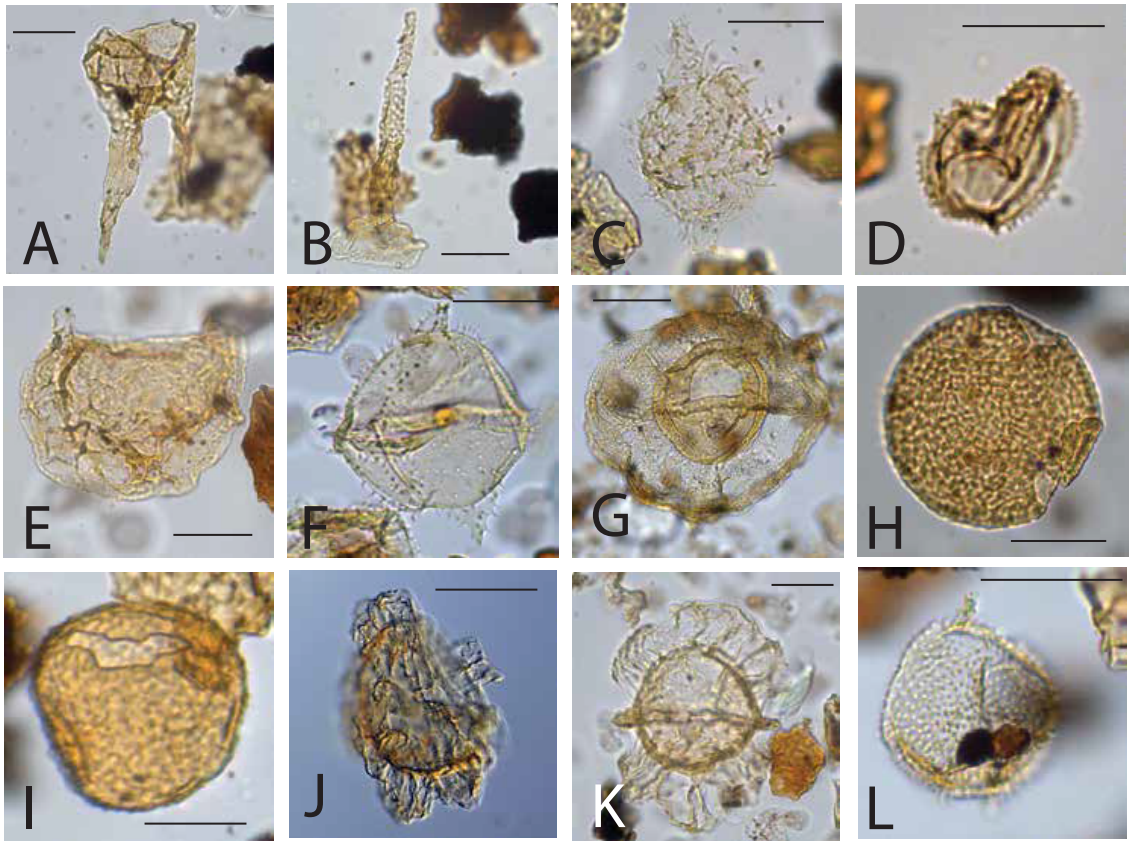
PLATE 2. A. *Odontochitina operculata*, FUEN1; **B.** *Odontochitina perforata*, FUEN1; **C.** *Palaeohystrichophora infusorioides*, FUEN1; **D.** Selenopemphix brinkhuisii Bijl *et al.*, 2018, PM8; **E.** *Senoniasphaera inornata*, FUEN3; **F.** *Spinidinium macmurdoense,* Río Los Palos (LP)14; **G.** Thalassiphora pelagica, SELK65-7-1-10; **H.** Trithyrodinium vermiculatum, FUEN3; **I.** Trithyrodinium vermiculatum, FUEN3; **J.** *Turbiosphaera filosa*, T-1-20-2-70; **K.** *Turbiosphaera sagena*, LP14; **L.** *Vozzhennikovia apertura*, LP4. Scale bar=25 µm.